7

Activity Recognition

Wearable ECG recorders (W-ECG) provide a practical solution for ambulatory cardiac monitoring. W-ECGs are increasingly being used by people suffering from cardiac abnormalities, who also choose to lead an active lifestyle. From the discussions in the previous chapters regarding W-ECG, we can now understand that the challenge presently is that the ambulatory ECG signal is influenced by motion artifacts induced by body movement activity (BMA) of the wearer. The usual practice is to develop effective filtering algorithms which can eliminate the motion artifacts. However, due to spectral overlap between the motion artifact signal and the cardiac signal the complete elimination of the motion artifact from the ambulatory ECG signal is not possible without unduly affecting the cardiac signal component. Therefore, instead of filtering we would like to identify the presence of the motion artifact and the type of body movement from the analysis of the ambulatory ECG signal itself. We have already addressed the issue of detecting BMA transitions from the ECG signal in the previous chapter. The method proposed for the transition detection is an unsupervised learning approach which only looks for any abrupt changes in the nature of the motion artifact signal due to changes in BMA. However, a particular BMA is not yet characterized from the analysis of ECG in the previous chapter. In this chapter we focus on the BMA recognition from the ambulatory ECG signal for which we will use BMA classifiers with certain specific types of BMA classes. The classification approach for BMA recognition requires supervised training of the specified BMA classes using the corresponding ECG data during the specified BMA. For this purpose we have recorded the ECG signals during specified BMA, e.g. sitting still, walking, movements of arms and climbing stairs, etc. with a single-lead W-ECG as described in Section 5.2. The collected ECG signal during the BMA is presumed to be an additive mix of signals due to cardiac activities, motion artifacts and sensor noise as per the mathematical model given in Section 1.5. We have successfully used the mathematical model of the ambulatory ECG in the previous chapter for the transition detection from the ambulatory ECG signal. Here we follow the same model of the ambulatory ECG signal for the

S. Chaudhuri et al., *Ambulation Analysis in Wearable ECG*, DOI: 10.1007/978-1-4419-0724-0_7, 79

analysis which leads to the recognition of different types of BMA from the ECG itself. According to the mathematical model, the motion artifact signal is one of the components of the ambulatory ECG signal which depends on the type of BMA and hence the BMA recognition should be possible from the analysis of the ECG signal. The motion artifact signal can be derived from the ambulatory ECG by suppressing the cardiac signal and the sensor noise. We hypothesize that a similar type of BMA induces a similar type of motion artifact whereas different types of BMA induce different types of artifact. If this is true then we can train a classifier to detect the type of BMA class using the motion artifact signal. As per the mathematical model in Section 1.5, we first derive the motion artifact signal by estimating the cardiac signal. The derived motion artifact signal can be used for the BMA recognition. We use classifiers trained for different BMA classes in which there are two types of representations: one is a nonparametric representation and the other is a parametric representation. In the nonparametric BMA classifiers each of the BMA classes is represented by a set of vectors derived from the ambulatory ECG data for the specific BMA class during training. Whereas in the parametric BMA classifiers, the individual BMA class is modeled by certain parameters derived from the ambulatory ECG data available for only that particular BMA class. Both kinds of representations obtained by the supervised learning are then used for classification of the ambulatory ECG signals to recognize the BMA class during testing. Here we use the derived motion artifact signal for supervised training of the BMA classifiers and the classification of BMA types, which requires some preprocessing on the ambulatory ECG signals recorded by W-ECG. The details of preprocessing and analysis are presented in this chapter.

7.1 Introduction

The ECG signal collected by the W-ECG is contaminated by BMA induced artifacts owing to disturbances at the skin electrode interface and noise due to muscular activities, collectively known as motion artifacts. For the W-ECG to handle motion artifacts occurring naturally during its intended use is a challenge. The motion artifacts have a significant overlap in frequency with ECG signal, so filtering based on spectral separation is of limited use [5].

In the earlier chapters we have provided a brief introduction to the problem of motion artifact in W-ECG. Any body movement activity (BMA) of the wearer causes motion artifacts and we have shown from the BMA transition detection in the previous chapter that different types of BMA induce different kinds of motion artifact. Using the BMA transition detection method, it is possible to segment the ECG signal temporally in order to separate each of the signal segments containing just one type of BMA. Since BMA influences the ECG output, we propose to determine the BMA from the motion artifacts in the ECG signal. The possibility of recognition of the BMA from ECG data

is yet to be fully studied in the literature. We also show that BMA recognition can help in improving the automated analysis of the ambulatory ECG signal in W-ECG. This will be helpful eventually in pervasive monitoring of cardiac activity of a patient and determining if any BMA is having a deleterious effect. The possibility of such a classification has initially been explored in [93]. Here the ECG signals are analyzed using a wavelet transform and a neural network. However, the reported performance is not very satisfactory as the wavelet based representation does not separate the in-band BMA signal from the ECG. In other works related to BMA analysis from non-ambulatory ECG, body position changes are detected for ischemia monitoring in [9, 37, 52]. In [37, 52], Karhunen-Loeve transform of the ECG beats are analyzed to detect position changes. A synthesized vectorcardiograph based approach has been proposed in [9, 37], where a series of angles for the three orthogonal leads X, Y and Z are derived using a loop alignment method [9, 122]. The sequence of angles is then analyzed to detect the changes in body position. However, this method requires a comprehensive 12-lead ECG signal to be able to synthesize the three vectorcardiograph leads and is currently restricted to a clinical environment. The single-lead system that we have used is less informative but enables long term cardiac monitoring and is also preferable from the standpoint of wearer's comfort and cost.

In this chapter we characterize the motion artifacts induced by the following specific BMAs: sitting still, up and down movement of left, right and both arms, walking on a level floor, and climbing stairs up and down, using two different supervised learning approaches. In the first approach we use a non-parametric classification technique based on principal component analysis (PCA). The second approach is a parametric classification technique based on hidden Markov models (HMM). In both the approaches we test for classifiability of the motion artifacts based on the characterization obtained using the supervised learning. For this purpose we build various BMA classifiers for different BMA classes where each class is either a distinct BMA or a combination of two or more different BMAs as specified above. If two specified BMAs are not quite separable using the proposed characterization of motion artifacts, they are both combined into a single BMA class. Here we demonstrate that it is indeed possible to recognize several BMA classes accurately from the ECG signal itself. Since the proposed non-parametric classification technique is based on the PCA of motion artifacts in the ECG signal, it follows that class specific PCA-based filtering can also be used for removal of motion artifacts. Accordingly, we have demonstrated the usefulness of the PCA-based filtering technique by locating the P and T waves in the ECG signal in the presence of body movement.

Here we have restricted our studies to only people with no known cardiac abnormalities but under multiple settings (laboratory and outdoors). Since the motion artifact is caused at the superficial level at the skin, it is understood that the possibility of the BMA recognition shown here for the healthy subjects should also be applicable for cardiac patients except the fact that the

proposed PCA-based method may not be suited for cardiac patients with frequent rhythmic disturbances. However, for patients with infrequent rhythmic disturbances, it is possible to detect such abrupt episodes using the RPCA method proposed in the previous chapter following a post-processing step of arrhythmia classification using some standard method.

The organization of the chapter is as follows. We discuss a nonparametric, supervised learning-based classifier using PCA in Section 7.2. There we discuss the mathematical model for the ambulatory ECG signal recorded by the W-ECG, required preprocessing steps for implementation of the proposed method on ECG signal, basics of PCA, supervised learning and classification of BMA. We also explain how the BMA classification can be used for removal of the motion artifacts. We explain a parametric, supervised learning-based classifier using hidden Markov models (HMM) in Section 7.3. The results of the BMA classification obtained by the two algorithms are presented in Section 7.4. We discuss about the conclusions of our experiments on BMA recognition from ambulatory ECG signal in Section 7.5.

7.2 Nonparametric Classification

According to the mathematical model of the ambulatory ECG signal given in the earlier chapters, the recorded ECG signal has three components: cardiac signal due to normal heart activity, motion artifacts due to body movement and sensor noise introduced by the W-ECG. Following the BMA transition detection results presented in the previous chapter and some preliminary results regarding BMA recognition using the wavelet based method in [93], we hypothesize that each type of body movement induces a particular type of motion artifacts in the ECG signal. An ECG signal for the i^{th} class of BMA is modeled as

$$r_i(n) = q_i(n) + s_i(n) + \eta(n), \tag{7.1}$$

where r_i is a recorded ECG signal, q_i is a cardiac signal of a normal heart during BMA specified by i^{th} class, s_i is an additive motion artifact due to i^{th} class of BMA and η is the sensor noise present in the ECG signal. It is noted that the cardiac cycle q_i is denoted for the specific BMA to emphasize that the cardiac cycle can be more accurately represented and estimated when considered separately for an individual BMA class.

Here we discuss a nonparametric approach of classification for recognition of BMA from the ambulatory ECG signal based on principle component analysis (PCA) technique. We segment the ambulatory ECG signal contiguously as a sequence of ECG beats. Each of the ECG beats in the sequence will be represented as a vector of a fixed dimension for the PCA-based analysis for BMA recognition.

Let the vector representations of the corresponding signals captured during a single period of heart beat be $\underline{r}_i$, $\underline{q}_i$, $\underline{s}_i$ and $\underline{\eta}$, respectively. All vectors used for

the classification are column vectors. As mentioned earlier, the dimension M_0 of these vectors depend on the beat period and the sampling frequency. If one considers N consecutive heart beats together as a signal then the dimension of the signal would be $N\dot{M}_0$. Following are the various assumptions made while developing the nonparametric PCA-based classifiers.

1. The cardiac signal q_i is assumed to be representing normal cardiac activity only and it remains stable in the presence of a specific BMA.
2. Since cardiac activity is by nature involuntary, it is independent of voluntary muscular activities and motion of electrodes. Hence BMA induced motion artifacts s_i are independent of the cardiac signal q_i, i.e., $q_i \perp s_i$.
3. The sensor noise η present in the ECG signal is due to ambient conditions of recording like power line interference, device temperature, skin humidity, etc. and, therefore, it is assumed to be independent of both cardiac signal and the motion artifact, i.e., $\eta \perp q_i$ and $\eta \perp s_i$.
4. In the preprocessing steps described next (Section 7.2.1), the dc bias estimated from the isoelectric level of the ECG signal is set to zero. Therefore, the sensor noise is assumed to be of zero mean, i.e., $E[\underline{\eta}] = 0$.
5. $\text{Rank}(E[\underline{r}_i \underline{r}_i{}^T]) \approx M_i$, where $M_i \leq M_0$, signifying that the actual information in the recorded ECG signal can be compactly represented by only top M_i eigenvectors.
6. The energy of the motion artifact signal s_i is concentrated into a top few (say K_i where $K_i \ll M_i$) eigenvectors of $E[\underline{s}_i \underline{s}_i{}^T]$, and that the composite signal $\underline{r}_i$ is sufficiently excitatory.
7. There is greater correlation between signals due to same type of body movement than that for any two different types of body movement. That is, s_i and s_k are highly correlated if $i = k$ (at different time instants) and nearly uncorrelated if $i \neq k$.
8. The signal component due to motion artifacts is smaller compared to the strength of the cardiac signal, but much greater than the sensor noise, i.e., $|\underline{\eta}| \ll |\underline{s}_i| < |\underline{q}_i|$, $\forall i$.

Based on the mathematical model and the assumptions discussed above, we will extract the signature of a specific BMA (s_i) by eliminating the cardiac signal (q_i) and the sensor noise (η).

The cardiac signal is characterized by a stable rhythm of heart beats. Following assumption (1), the cardiac rhythm stays nearly constant over the heart beats within the observation window. An arithmetic mean of several epochs of heart beats provides an estimate of the constant cardiac rhythm and hence the cardiac signal [5, 49]. For a specific BMA class, this estimate is averaged over the entire training data set for a particular class and is termed as class mean of the BMA. If the class mean is a correct estimate of the cardiac signal then according to Eq. (7.1), the motion artifacts component (also sensor noise) is derived by removing the class mean from the ECG signal.

The sensor noise component is suppressed by elimination of the dc bias during the preprocessing step described next. Accordingly, the motion artifacts component will dominate as per assumption (8).

In the nonparametric classification, an unknown ECG beat is classified into a specific BMA class according to the best reconstruction criterion. A particular BMA class is represented by a set of top few eigenvectors of the training BMA data belonging to that BMA class. The eigenvectors are obtained from eigen decomposition of the correlation matrix of the training BMA data. The test ECG beat is reconstructed using the set of eigenvectors in conjunction with the class mean for each BMA class. The BMA class for which the error between the reconstructed signal and the test ECG beat is minimum is determined as the true BMA class for the unknown ambulatory ECG data.

The eigen decomposition technique described above is optimal for the assumed data representation model because the eigenvectors are orthogonal. Thus, after preprocessing, if the artifact signal (s_i) is corrupted by an uncorrelated noise signal (η) then the top few eigenvectors represent mostly the signal component due to BMA as the signal to noise ratio (SNR) is considered to be high in these components and the remaining eigenvectors mostly represent the noise subspace, thus isolating the BMA signal from noise.

Thus the method applied here is a nonparametric supervised technique for body movement classification. However, in order to be able to use the technique and for suppressing the sensor noise η, certain preprocessing steps are required to handle both intra-personal and inter-personal variations in the cardiac signal (q_i).

7.2.1 Preprocessing

It is assumed that the heart is not stressed during the activities that are being performed in this study. However, certain parameters like the coupling between skin and electrodes, and the variability in the heart rate have multiparameter dependence. The coupling between skin and electrodes depends mostly on the skin humidity levels and also if the setting is indoors or outdoors. Similarly, a small variation of heart rate during ambulatory activity is present even in healthy subjects. Finally, there are person specific variations in the above two parameters. While the coupling between skin and electrodes affects the amplitude (scale) of the ECG beat data, the heart rate affects the time interval of the ECG beat data.

The arithmetic mean as an estimate of the cardiac signal ($\underline{q}_i$) and eigen decomposition for extraction of the motion artifact component ($\underline{s}_i$) are both sensitive to translation, variations in amplitude and time scales of the data [52]. Thus it is necessary to perform the following preprocessing steps that involve proper alignment, amplitude scaling and time warping of the data as shown in Fig. 7.1.

The data is processed as a batch of ECG beat epochs collected over about one minute duration after appropriate beat alignment. This implicitly assumes

that the collected beat epochs in this short time duration, may have nearly constant amplitudes and time periods.

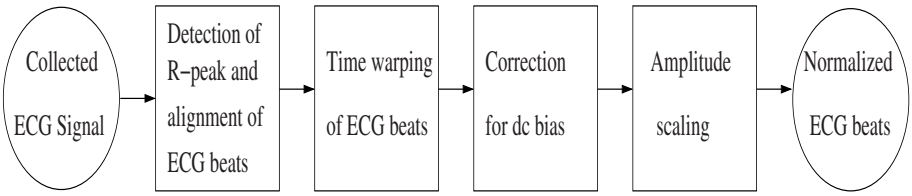

Fig. 7.1. Preprocessing applied to the ECG signal captured by the W-ECG. (©2007 IEEE)

Detection of R peak and alignment of ECG beats

The R peak is the most prominent feature of the ECG signal that can be detected easily even in the presence of motion artifacts, and is used for calculating the heart rate. The R peaks in the ECG signals are detected using the Pan-Tompkins method [96]. The method for detection of R peaks in ECG has been explained in the previous chapter. The duration between the current R peak and the preceding one is considered as the current ECG beat interval, i.e., j^{th} beat interval is given by duration between $(j-1)^{th}$ and j^{th} R peaks. The average interval of the ECG beats is estimated from the number of R peaks detected over a period of one minute. If there are a total of N ECG beats over the given period then the ECG signal is partitioned into N ECG beat epochs. The R peak in each epoch is aligned to the exact middle position. This strategy ensures the alignment of ECG beats even after time warping is applied to the data.

Time warping of ECG beats

As explained above, the ECG beat intervals may vary due to change in the heart rate. Accordingly, the number of samples recorded for each ECG beat epoch may vary. Since the given PCA-based method is applicable only to vector observations in a space of fixed dimension, it is required to equalize the dimensions (M_0) of all the ECG beats. A simple technique to achieve this is linear time warping and is implemented as follows. The ECG beat is resampled by a rational factor a/b, where a is the fixed number of samples after the time warping, and b is the number of samples in the ECG beat being resampled. This is performed through MATLAB® using a polyphase implementation of resampling and a linear phase anti-aliasing filter with finite impulse response. Following the application of time warping, all the ECG beat observations are of equal length.

Correction for dc bias

The constant voltage level of the flat portion of ECG beat segment that lies between the end of P wave and the beginning of Q wave is termed as the isoelectric level of the ECG beat [49]. Ideally, the isoelectric level should be at ground potential. The dc bias is estimated by calculating the arithmetic mean of isoelectric levels of all ECG beat observations collected during a one minute interval. This dc bias is then subtracted from the ECG signal. Thus any dc bias introduced due to sensor noise or otherwise is removed during this step. The shape of the recorded ECG signal remains unchanged at this point of time and the sensor noise in ECG signal has now zero mean as per assumption (4).

Amplitude scaling

This is the last stage of preprocessing. As discussed earlier, the coupling between skin and electrodes can affect the amplitude of the signal. Since the proposed method calculates the arithmetic mean of the ECG beats for estimating the cardiac signal component, all the ECG beats should represent the cardiac activity with the same amplitude. The R wave peak with respect to the isoelectric level is considered here to represent the full signal strength. A normalization factor is estimated by averaging of R wave amplitudes with respect to the corresponding isoelectric levels from all ECG beats over a period of one minute. Thus the amplitude of the ECG data over the period is normalized and the estimate of average R wave amplitude with respect to the corresponding isoelectric level becomes unity.

7.2.2 Principal Component Analysis (PCA)

We propose to use a nonparametric classification technique for recognition of BMA from the ECG signal. Since we focus in this work on W-ECG devices which may provide only a single lead ECG signal at a time, we choose a technique for a suitable nonparametric representation of the signals. The technique we consider here is known as PCA. Here the data set is organized in such a way that each point in the data lies in a fixed dimensional space and each element of the data is along a specific orientation (axis) in the space. That is to say that each data can be represented as a vector in the fixed dimensional space. In this representation let M be the fixed dimension of the space and the data be represented in a column vector form of dimension $M \times 1$. Thus the complete vector space can be defined by a basis which is a set of independent vectors in $\Re^M$. Since the dimension of the vector space is M, there must be at most M such independent vectors in the basis. Each of the elements in the column vector is the projection corresponding to a basis vector in an ordered manner.

The PCA is a technique used for finding the most suitable bases to represent the given data. This is because there may be some redundancy in the data and therefore, the dimension can be reduced. In this case the bases would be such that even a few of the vectors from the bases can represent the data satisfactorily without much loss in terms of the errors in reconstruction. Using PCA the vectors forming such bases can be found in an ordered manner. Here the vectors found by the PCA are called eigenvectors which are orthogonal to one another and also normalized to yield the signal power of each vector to be unity. Therefore, one can say the derived bases form an orthonormal set of bases. There is no redundancy in this representation due to the orthogonality of the basis. Moreover, the eigenvectors are found in such a manner that the first eigenvector captures the maximum signal power in the data along any direction. The next eigenvector will be in an orthogonal direction to the previously found eigenvector(s) that captures the next highest amount of signal power from data along all other possible (orthogonal) directions. According to the signal power captured by each of the eigenvectors, it is assigned an eigenvalue which represents the weight of the particular eigenvector for the given data. Thus the eigenvectors are arranged in a non-ascending order of eigenvalues. In most practical applications the first few eigenvectors are able to capture most of the signal power in the data and the remaining eigenvectors only represent a small residual which is either considered as noise or can be neglected without much loss in data reconstruction. Thus a graceful tradeoff between the number of eigenvectors and the loss in data reconstruction is achieved using the PCA.

Let a set of data contain a total of N observation points from a fixed dimensional space, $\underline{r}_i(n)$, $i = 1, 2, \ldots, N$ observations where $\forall \underline{r}_i(n) \in \Re^M$. Here M is the fixed dimension of the space under consideration. We want to apply PCA to the given data set.

First, the data set is centered to zero by subtracting the arithmetic mean of the data. The arithmetic mean of the original data is computed as

$$\overline{\underline{r}} = \frac{1}{N} \sum_{i=1}^{N} \underline{r}_i. \tag{7.2}$$

The corresponding vector after mean subtraction is denoted by $\underline{r'}$ where

$$\underline{r'}_i = \underline{r}_i - \overline{\underline{r}},\ i = 1, 2, \ldots, N. \tag{7.3}$$

The covariance matrix is computed from the mean subtracted data as

$$C = \frac{1}{N} \sum_{i=1}^{N} (\underline{r'}_i)(\underline{r'}_i)^T, \tag{7.4}$$

where C is the covariance matrix for the given data and $(\cdot)^T$ is matrix transpose. Here C is an $M \times M$ matrix and its eigen decomposition gives a total of

M eigenvectors $[e_1, e_2, \ldots, e_M]$, arranged in a non-ascending order of the corresponding eigenvalues, denoted by $\lambda_1 \geq \lambda_2 \geq \ldots \geq \lambda_M$. For details of eigen decomposition the interested reader may refer to [38]. Let $E = [e_1, e_2, \ldots, e_K]$, $K \ll M$ be a set of first K eigenvectors with the largest eigenvalues that represents a smaller K dimensional subspace in the M dimensional space of the given data. In many practical applications a suitable choice of K will yield an almost perfect reconstruction with a very small residual error. Hence the PCA technique is used for reducing the dimensionality of the given problem. Moreover, in most cases the residual errors are from the noise subspace which one would like to suppress from the data. Therefore, the PCA is also used for noise removal.

The dimensionality reduction helps to shrink certain useful subspaces in the data which characterize the conditions under which the observations are recorded. We may expect that the corresponding subspaces derived from different data sets recorded under different conditions will be quite separate. This separation of subspaces for different conditions may help to solve the classification problem. One can first derive the corresponding subspace from the training data given for each specific pre-defined condition and then try to find the distance of a test data from the derived subspace. The point may be allocated the condition (or class) represented by the nearest subspace. However, the PCA itself does not guarantee the separability of the subspaces and hence it is not necessarily always the preferred technique for solving the problem of classification. For details of various techniques of classification, the interested reader may refer to [24]. For certain types of data the PCA can indeed be applied successfully for classification purposes. We discuss a technique based on PCA for BMA recognition from the ECG signal in this chapter.

7.2.3 Supervised Learning of Body Movement

Following the mathematical model of the ambulatory ECG signal adopted for the analysis, the ECG signal comprises of the cardiac signal (q_i), motion artifacts (s_i) and sensor noise (η). The ECG beats segmented after the preprocessing will be considered for training and subsequent classification of BMA. As explained above, the vector representation of the j^{th} ECG beat observation in the training data of i^{th} BMA class is $\underline{r}_{ij}$ and the vector representations of the corresponding cardiac signal, motion artifact and sensor noise components are $\underline{q}_{ij}$, $\underline{s}_{ij}$ and $\underline{\eta}_{ij}$, respectively.

We plan to use a supervised approach of training a BMA classifier using the processed ECG beat, $\underline{r}_{ij}$, $i = 1, 2, \ldots, c$ and $j = 1, 2, \ldots, N_i$, where c is the number of BMA classes in a classifier and N_i is the number of ECG beats used for training of i^{th} BMA class. In this nonparametric classification approach each BMA class is represented by a class mean and a set of eigenvectors computed using the PCA of all training observations. The class mean is computed from the arithmetic mean of the training data $\underline{r}_{ij}$, $j = 1, 2, \ldots, N_i$

of the i^{th} BMA class. The eigenvectors for the BMA class are obtained from the corresponding data after subtracting the class mean.

The class mean of i^{th} BMA class is calculated as follows

$$\widetilde{\underline{q}}_i = \frac{1}{N_i} \sum_{j=1}^{N_i} (\underline{r}_{ij}), \tag{7.5}$$

which approximates the average cardiac signal for the given BMA class [49]. The average cardiac component $\widetilde{\underline{q}}_i$ is subtracted from the signal $\underline{r}_{ij}$ to derive mean subtracted BMA vectors (residual signal) for the i^{th} BMA class

$$\underline{r'}_{ij} = \underline{r}_{ij} - \widetilde{\underline{q}}_i \simeq \underline{s}_{ij} + \underline{\eta'}_{ij}, \tag{7.6}$$

where $\underline{\eta'}_{ij}$ is comprised of the sensor noise plus the noise arising in the estimation of the cardiac component due to inter-personal variation (refer to multi-subject testing, classifiers VI-X in Section 7.4.1). The BMA vectors with regards to signal power, contain predominantly the motion artifact $\underline{s}_{ij}$, along with the noise $\underline{\eta'}_{ij}$.

Next, PCA is applied on the BMA vectors $\underline{r'}_{ij}$ to compute the significant eigenvectors of the training data for each BMA class. An eigenvalue corresponding to an eigenvector is a measure of signal strength in the data in the direction of the eigenvector. As per assumption (8), the motion artifact component dominates the residual signal. Thus, if the eigenvectors of this data are arranged in a non-ascending order of the respective eigenvalues, the first few eigenvectors will represent the motion artifacts by neglecting the noise components. For the i^{th} BMA class, the eigenvectors and eigenvalues are computed by eigen decomposition of the covariance matrix of the training residual signal $\underline{r'}_{ij}$, given by

$$C_i = \frac{1}{N_i} \sum_{j=1}^{N_i} (\underline{r'}_{ij})(\underline{r'}_{ij})^T, \tag{7.7}$$

where C_i is the covariance matrix for the i^{th} BMA class. If the data occupies an M dimensional space then C_i is a $M \times M$ matrix and its eigen decomposition gives a total of M eigenvectors $[e_{i1}, e_{i2}, \ldots, e_{iM}]$, arranged in the non-ascending order of the corresponding eigenvalues, denoted by $\lambda_{i1} \geq \lambda_{i2} \geq \ldots \geq \lambda_{iM}$ for the i^{th} BMA class. Let $E_i = [e_{i1}, e_{i2}, \ldots, e_{iK_i}]$, $K_i \ll M$ be a set of first K_i eigenvectors with the largest eigenvalues that represent the motion artifacts. Here E_i forms a basis for a small K_i dimensional motion artifact subspace in the M dimensional space of the data for the i^{th} class. As per assumption (7) the motion artifacts due to any two different types of BMA are nearly uncorrelated, eigen functions for any two different motion artifacts are also expected to be nearly uncorrelated.

For each BMA class, a class mean and a set of eigenvectors are computed from the training observations, which represent the characteristics of motion artifacts for the particular BMA and is used as the basis of the BMA classifier. Thus we have obtained a non-parametric representation of each BMA class.

7.2.4 Activity Classification

Based on the nonparametric representation obtained in the previous section for each of the specified BMA classes in a classifier, we discuss a BMA classification procedure in this section. Let $\underline{p}_u$ be a test ECG beat extracted after the preprocessing steps given in Section 7.2.1, where u is the label of the BMA class of $\underline{p}_u$ which is unknown to the BMA classifier but can be any one of BMA class labels $i = 1, 2, \ldots, c$; where c is the total number of BMA classes in the classifier. To classify $\underline{p}_u$, i.e., to recognize the class label u, the following procedure is applied. First, the corresponding class mean $\widetilde{\underline{q}}_i$ is subtracted from $\underline{p}_u$ for all the BMA classes $i = 1, 2, \ldots, c$ to get

$$\underline{p'}_i = \underline{p}_u - \widetilde{\underline{q}}_i, \tag{7.8}$$

where $\underline{p'}_i$ is a mean subtracted residual BMA vector for the candidate i^{th} BMA class. The BMA vector $\underline{p'}_i$ is reconstructed from projections on the computed set of eigenvectors E_i to capture its contents in the i^{th} motion artifact subspace defined by E_i in the prior training as

$$\widetilde{\underline{p'}}_i = (E_i E_i^T)\underline{p'}_i, \tag{7.9}$$

where $\widetilde{\underline{p'}}_i$ is the reconstructed i^{th} motion artifact.

A measure of error in reconstruction in i^{th} motion artifact is denoted by $error(i)$ and defined as

$$error(i) = |\widetilde{\underline{p'}}_i - \underline{p'}_i|^2. \tag{7.10}$$

To recognize the BMA class of the ECG beat, u is assigned the class label from $i = 1, 2, \ldots, c$ for which the error in reconstruction is the minimum

$$u = \arg\min_i error(i). \tag{7.11}$$

The above derivation is valid when one is trying to classify motion artifacts using the ECG signal for a single beat duration. However, one can have l number of consecutive ECG beats during a particular BMA. The use of l beats instead of a single beat can lead to a better classification accuracy. Hence, for the BMA classifier, the given method of classification can be generalized for a test sequence of l ECG beats $\{p\}_u = \{\underline{p}_{u1}, \underline{p}_{u2}, \ldots, \underline{p}_{ul}\}$, where $\underline{p}_{uj}$ is j^{th} test ECG beat and u is the single label for all the test ECG beats in the sequence. The error in reconstruction given in Eq. (7.10) for the test ECG beats $\underline{p}_{uj}$, is denoted by $error_j(i)$ for $j = 1, 2, \ldots, l$ in the given sequence. Finally, the following measure of error is computed

$$error(i) = \sum_{j=1}^{l} error_j(i). \tag{7.12}$$

The class label corresponds to i for which $error(i)$ is minimum.

7.2.5 Removal of Motion Artifacts

The classification procedure as derived above can also be applied to eliminate motion artifacts in ECG due to body movements. The BMA class for an ECG beat under test is recognized by the BMA classifier and the corresponding artifact components are removed. Let $\underline{p}_i$ be an ECG beat where i is the recognized BMA class, and the set of eigenvectors E_i represents the artifacts in $\underline{p}_i$ due to the recognized BMA. For artifact removal, the ECG beat is reconstructed by removing the components of the corresponding mean subtracted observation $\underline{p'}_i = \underline{p}_i - \widetilde{\underline{q}}_i$, in the artifact subspace spanned by E_i as

$$\widetilde{\underline{p}}_i = \underline{p}_i - (E_i E_i^T)\underline{p'}_i, \tag{7.13}$$

where $\widetilde{\underline{q}}_i$ is the class mean of the recognized BMA class as defined in Eq. (7.5) and $\widetilde{\underline{p}}_i$ is the reconstructed ECG beat. We expect such a signal to be more useful to clinicians. We demonstrate this by analyzing this signal to obtain more accurate results in the detection of P and T waves. This is given in Section 7.4.1.

7.3 Parametric classification

In the previous section we have discussed nonparametric classification of BMA from the ambulatory ECG signal. In this section we provide a very different approach of BMA classification. The parametric, supervised classification technique is based on hidden Markov models (HMM). Here we overcome some of the limitations in using the PCA-based technique discussed in the previous section. The ECG beat alignment procedure required in the PCA-based technique can distort the motion artifact signal if there is a significant variation in the heart rate. Here we prevent this situation by proposing an adaptive filter as a preprocessing step for separating the motion artifact signal from the ECG signal. The derived motion artifact signal is then processed further for classification of various types of BMA. The classification of BMA is performed using different HMMs for different BMA classes. Like the previously proposed PCA-based technique, this method is also a supervised learning based classification method. However, since the parameters of the HMM model are estimated from the training signals, the method is a parametric classification technique as opposed to the PCA-based method which is a non-parametric classification technique. At the end of this chapter we compare the BMA classification results obtained using both the methods. It is noted that the HMM-based method, though computationally a bit more expensive, outperforms the PCA-based method. However, this is predominantly a classification scheme as opposed to the PCA-based method which is a subspace based reconstruction scheme where artifact removal is obtained as a by-product. For the HMM-based method, once a BMA is recognized, the corresponding PCA for the class should be used if noise removal is required.

In the PCA-based method different sets of principal components and the mean cardiac cycle are computed from the training data to represent the corresponding BMA classes. The PCA-based method provides a good dimensionality reduction and can be applied even when only a single-lead ECG signal is available. However, the PCA-based method requires alignment of cardiac features for separation of cardiac and motion artifact signal subspaces. The problem of alignment is partially solved by resampling of the ECG beats in accordance with the heart rate. However, the resampling process introduces artifacts in the QRS complex and distortion in the spectra of the motion artifact signal. Since the cardiac cycle in PCA is computed from the average of time-warped ECG beats, the artifacts caused due to resampling of the QRS complexes, also affect this estimate. The severity of the distortion is proportional to the amount of resampling, which is determined by the variability of the heart rate. Due to this reason the method is restricted to the cases where the heart rate variability in the individual BMA class is not significant. Therefore, it is necessary to devise a new method for BMA recognition, in which this kinds of distortion can be prevented.

To circumvent the problems due to resampling, we separate the motion artifact signal from the ECG initially using an adaptive filter. This is done in order to suppress any cardiac signal components which are common in all types of BMA and which may overwhelm the modeling effort by the HMM, and hence may not help in the BMA classification. We assume that since each BMA is performed in a different manner the spectral features of the motion artifact signal will exhibit some specific kind of temporal behavior. If this assumption is true then the specific temporal characteristic can be modeled using an HMM for each individual BMA class. The time-localized features derived from spectral energy of the motion artifact signals can be computed for each specific BMA class using Gabor filters and they will be simply referred to as Gabor features from here on. The details of computing the Gabor features from the motion artifact signals will be explained later in this chapter.

We explore the feasibility of BMA recognition using HMM, which is considered here also due to its inherent temporality [24, 106]. For this purpose, parameters of an HMM for each BMA class will be determined by using a supervised learning approach, from the Gabor features of the corresponding motion artifact signals reserved for training. The parameters of an individual HMM are initialized by random choice and then updated for maximizing the likelihood of the data from the corresponding BMA class during this training. After the training, all the HMMs with known parameters will be used for calculating likelihood of each of the data provided for testing. The BMA class of the test data is recognized based on the maximum likelihood criterion over all the trained HMMs. The details of the implementation of the adaptive filter, Gabor feature extraction and the HMM-based classification method are provided in the following subsections.

7.3.1 Pre-processing

The ECG signal acquired during a specific BMA is contaminated by the induced motion artifact signals. Preprocessing is required to separate the motion artifact signals from the composite ECG recordings. This is required so that the HMM can be trained on the artifact signal alone and the training is not overwhelmed by the dominant cardiac signal. We use an adaptive filter that is conceptually similar to the adaptive recurrent filter (ARF) given in [130] for cancellation of motion artifacts.

In [130], an ARF is provided to obtain the impulse response $\underline{w}$ of the desired signal spanning over a fixed length M_0. In this case the desired signal is the recurring cardiac cycle (P-QRS-T complex) in the ECG signal which should be estimated by the filter impulse response $\underline{w} = [w_1\ w_2\ \cdots\ w_{M_0}]^T$. An impulse train is used as an input to the ARF, in which an impulse (unit sample) occurs at a specified point of each cardiac cycle (ECG beat). This specific point should preferably be at the starting of the ECG beat. This can be determined from the location of the R peak in the particular ECG beat. The length of the filter should be the same as the length of the ECG beat in order to estimate the complete cardiac cycle. The k^{th} filter coefficient w_k is adaptively modified by a least mean squares (LMS) algorithm at the incidence of the k^{th} sample of the current cardiac cycle based on the error between the k^{th} sample and the filter output.

Though the ARF, given in [130] is able to capture the cardiac cycle effectively, it is sensitive to the time synchronization of the impulses at the specified starting points of the cardiac cycles. Since the starting point is determined with respect to the R peak of the cardiac cycle the method is very sensitive to any error in locating the R peaks, which is likely to occur in presence of noise.

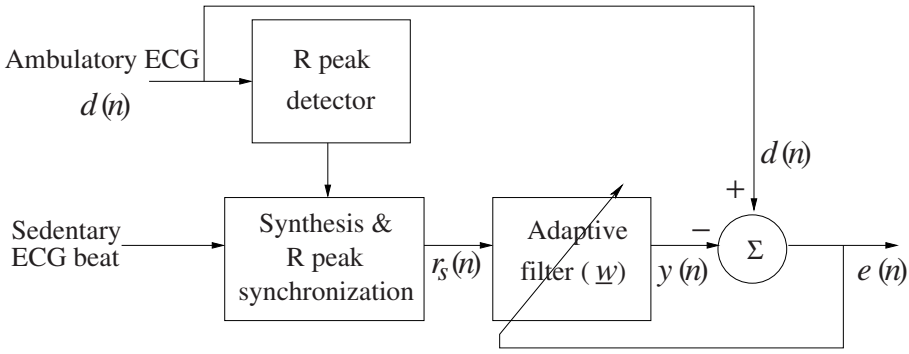

Fig. 7.2. A block diagram of the adaptive filter inspired by the ARF, given in [130].

Here in order to estimate the cardiac cycle more robustly we use a conventional adaptive filter [141] in which, as opposed to the ARF, all the filter

coefficients $\underline{w} = [w_1\ w_2\ \cdots\ w_N]^T$ are adaptively modified simultaneously at every sample. A block diagram of the adaptive filter is given in Fig. 7.2. A reference signal $r_s(n)$ is synthesized from a noise free ECG beat. This noise free ECG beat is acquired while the subject is in a sedentary condition. Next, the reference beat length is equalized with the current ECG beat length $r(n)$ such that the R peak positions of both the beats are perfectly aligned. This time synchronization of the R peaks of both the signals is performed by the synthesis block based on the R peak locations detected in the ambulatory ECG signal $r(n)$ using the R peak detector block. Thus the synthesized reference signal $r_s(n)$ exhibits the same heart rate as that of the ambulatory ECG signal $r(n)$ and the R peaks of both the signals are aligned. The coefficients of adaptive filter $\underline{w} = [w_1\ w_2\ \cdots\ w_N]^T$ are updated by the LMS algorithm given in [141] using the error signal $e(n)$ computed as the difference between the desired signal $r(n)$ and the filtered signal $y(n)$. The weights at n^{th} instant are updated using the error $e(n) = r(n) - y(n)$ as

$$\underline{w}_{n+1} = \underline{w}_n + \mu e(n)\underline{x}_n, \tag{7.14}$$

where $\underline{x}_n = [r_s(n-N+1)\ \ r_s(n-N+2)\ \cdots\ r_s(n)]^T$ is an input vector to the filter at n^{th} instant, μ is a parameter controlling the adaptation and convergence rate of the LMS algorithm, and N is the length of the filter. After the convergence, the adaptively filtered signal $y(n)$ estimates the desired cardiac signal component of the acquired ambulatory ECG signal $r(n)$ and the error signal $e(n)$ approximates the motion artifact signal $s(n)$.

It may be noted that for all the BMAs considered in this experiment, the quality of the acquired ECG signals from lead-II, despite the presence of motion artifacts, was such that it allowed a reliable detection of the R peak using the Pan-Tompkins algorithm [96]. Fig. 7.3 illustrates the cleaning of ECG signal acquired during a twisting at waist activity performed by a subject. The acquired ECG signal is depicted in Fig. 7.3(a). The cleaned ECG signals by the given adaptive filter and the ARF discussed in [130] are shown in Fig. 7.3(b) and Fig. 7.3(c), respectively. The filtered ECG signals are representatives of the cardiac signal component of the acquired ECG signal which is contaminated by the motion artifact. The P-QRS-T complex is clean and clearly visible in both the filtered ECG signal. The signal obtained by the adaptive filter has the P-QRS-T complex similar to that obtained by the ARF method [130]. Moreover, the length of the P-QRS-T complex is not required to be fixed in the given adaptive filter. Therefore, it can handle variation in the heart rate in an automated manner. Thus we obtain a good estimate of the cardiac signal component from an ambulatory ECG signal contaminated by motion artifact. However, the quality of the signal has not yet been examined for its use in clinical purposes. The filtering is performed just for obtaining the motion artifact signal $s(n)$ for further analysis of ambulation in this study.

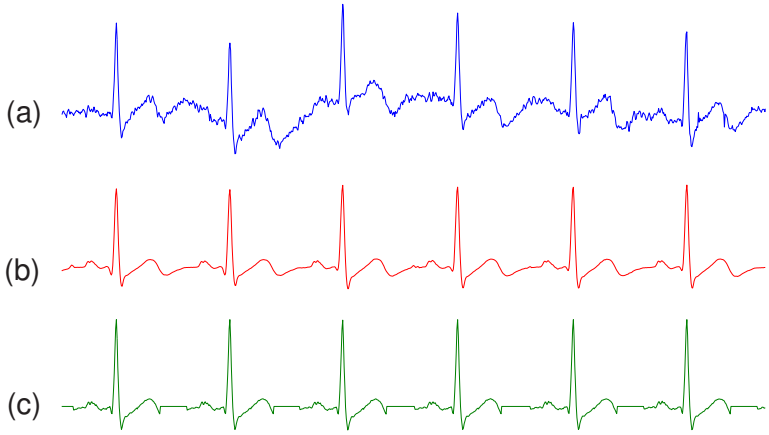

Fig. 7.3. Illustration of cleaning of ECG signal. (a) Original ECG signal while twisting at waist, computed ECG signal obtained with (b) the scheme of using noise free ECG beat reference, and (c) the ARF method in [130].

7.3.2 Feature Extraction

While preprocessing, an adaptive filter for obtaining the motion artifact signal $s(n)$ from the acquired ECG during a BMA is discussed. Since we are planning to use temporal relations among time localized frequency features for the modeling, the motion artifact signal $s(n)$ is analyzed into various subbands using Gabor filters. Gabor transform is known to have good time-frequency localization properties [36]. The different, equally spaced frequency components of the motion artifact signal $s(n)$ are computed by

$$\hat{s}_l(n) = e^{-\alpha^2(n/f_s)^2} e^{(j2\pi n l f_0/f_s)} * s(n), \tag{7.15}$$

where $*$ is convolution operator, f_s is sampling frequency, α, and f_0 are constant "sharpness" and "frequency" parameters [36], respectively, $\hat{s}_l(n)$ is a component of the motion artifact signal $s(n)$ and l is the index of a frequency component or subband. The envelopes of the impulse responses of the Gabor filters used for first three subbands are depicted in Fig. 7.4. The impulse responses span over 2 seconds and the center frequency lf_0 of the l^{th} subband filter increases proportionately to the value of index l, i.e., 1Hz, 2Hz and 3Hz, respectively for l= 1, 2 and 3 and f_0 = 1Hz.

Since the energies of the motion artifact signal are concentrated in 1-10Hz band, the number of subbands is selected through a suitable choice L to cover this frequency band, i. e., $l = 1, 2, \ldots, L$. An estimate of the energy in each of

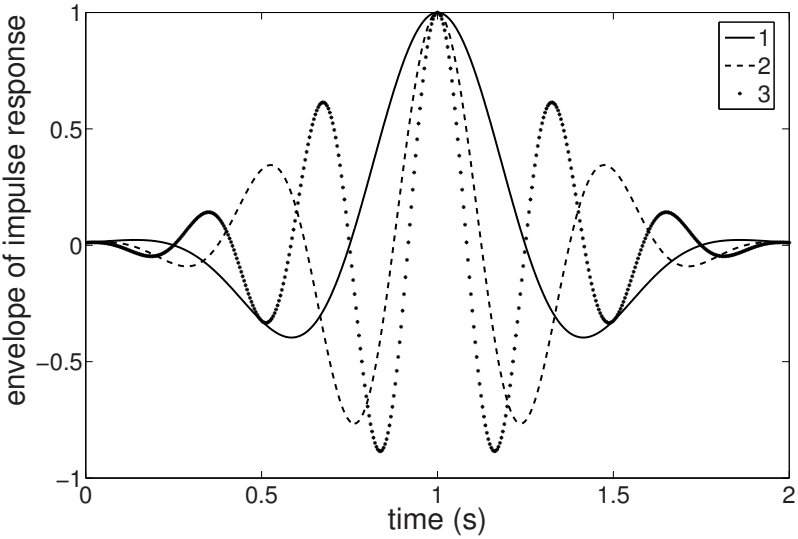

Fig. 7.4. Envelopes of the impulse responses of the Gabor filters used for first three subbands, l=1, 2 and 3.

these L frequency components $\hat{s}_l(n)$ is computed by a moving average of the windowed function as

$$g_l(n) = \frac{1}{W+1} \sum_{k=n-W/2}^{n+W/2} |\hat{s}_l(k)|^2, \tag{7.16}$$

where W is the width of the moving window. An example of the energy features for the analyzed signals in first four subbands is depicted in Fig. 7.5. It is noted that the signal power drops down with the increasing number of the subband.

For activity recognition, the feature vector $G(n) = [g_1(n)\, g_2(n)\, \ldots\, g_L(n)]^T$ is formed by L frequency components. This feature corresponds to the properties of the artifact signal at a given time instant. In order to consider the properties over a duration of N_0 consecutive samples, we put them as subsequent columns and construct the corresponding feature matrix

$$F(n, N_0) = [G(n - N_0 + 1)\; G(n - N_0 + 2)\; \cdots\; G(n)], \tag{7.17}$$

computed over N_0 contiguous samples of the motion artifact signal $s(n)$. This is used for the training and classification of BMA classes using an HMM-based technique. The dimension of the feature matrix $F(n, N_0)$ is $L \times N_0$.

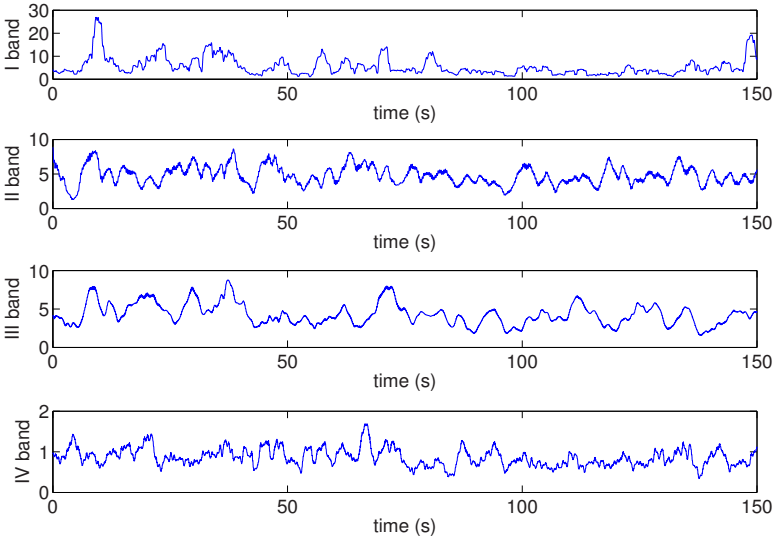

Fig. 7.5. Gabor feature signals $g_l(n)$, for first four subbands, l=1, 2, 3 and 4.

7.3.3 Hidden Markov Model (HMM) and Training

We provide an HMM-based classification technique for BMA recognition. In this technique, each of the BMA classes will be represented by an HMM. Since we are exploring the feasibility of using the HMM for BMA classification using the Gabor features derived in the previous section, we use the standard (also called fully connected or ergodic) HMM with finite mixtures of continuous observation probability density functions as given in [106]. To define the HMM, the number of states and the number of components in the mixture in each of the states are to be specified along with the associated parameters. For simplicity, we choose the same number of states in all the HMMs used for representing various BMA classes. Similarly, we choose the same number of mixture components for all the states. Let us denote the number of states in any HMM as $\mathcal{Q}$ and the number of mixture components in any state of the HMM as $\mathcal{M}$. The parameters of the HMM are:

- State transition probability $A = \{a_{ij}\},\ 1 \leq i \leq \mathcal{Q},\ 1 \leq j \leq \mathcal{Q}$, where a_{ij} is the state transition probability from i^{th} state to j^{th} state.
- Prior state probability distribution $\underline{\pi} = \{\pi_i\},\ 1 \leq i \leq \mathcal{Q}$, where π_i is the probability of the initial state of the system to be the i^{th} state S_i.
- Observation probability distribution $B = \{b_j\},\ 1 \leq j \leq \mathcal{Q}$, where b_j is a probability distribution for the observations when the system is in j^{th} state. The observation probability distribution for the j^{th} state b_j is modeled by a finite number of mixture components of continuous observa-

tion probability density functions with the mixture weight coefficients c_{jm}, mean vectors $\underline{u}_{jm}$ and covariance matrices Σ_{jm} for m^{th} mixture.

A finite mixture takes the form of the observation probability density b_j for the j^{th} state

$$b_j(G(n)) = \sum_{m=1}^{\mathcal{M}} c_{jm}\mathcal{N}(G(n)|\underline{u}_{jm}, \Sigma_{jm}), \tag{7.18}$$

where $G(n)$ is the observation being modeled, $\mathcal{N}$ is a Gaussian probability density with mean vector $\underline{u}_{jm}$ and covariance matrix Σ_{jm} for the m^{th} mixture component, and c_{jm} are mixture weight coefficients. The mixture weight coefficients c_{jm}, satisfy the conditions:

1. $\sum_{m=1}^{\mathcal{M}} c_{jm} = 1$, $1 \leq j \leq \mathcal{Q}$, and
2. $c_{jm} \geq 0$, $1 \leq j \leq \mathcal{Q}$, $1 \leq m \leq \mathcal{M}$.

In a short form the model is specified as

$$\Lambda = (\underline{\pi}, A, B), \tag{7.19}$$

where $\underline{\pi}$, A, and B are model parameters as defined above.

Let us define $\gamma_n(i)$, the probability of being in state S_i at an instant n given the model Λ and the observation sequence $F(n, N_0)$ defined in Eq. (7.17)

$$\gamma_n(i) = P(q_n = S_i|F(n, N_0), \Lambda), \tag{7.20}$$

where q_n is a variable indicating state at the instant n. Therefore, the probability of being in state S_i at instant n with the m^{th} mixture component accounting for the observation $G(n)$

$$\gamma_n(i, m) = \gamma_n(i)\frac{c_{jm}\mathcal{N}(G(n)|\underline{u}_{jm}, \Sigma_{jm})}{\sum_{m=1}^{\mathcal{M}} c_{jm}\mathcal{N}(G(n)|\underline{u}_{jm}, \Sigma_{jm})}. \tag{7.21}$$

Let us define $\zeta_n(i, j)$, the probability of being in state S_i at instant n and in state S_j at instant $n + 1$, given the model Λ and the observation sequence $F(n, N_0)$

$$\zeta_n(i, j) = P(q_n = S_i, q_{n+1} = S_j|F(n, N_0), \Lambda). \tag{7.22}$$

It has been shown by Baum *et al.* [13] that the probabilities $\gamma_n(i)$, $\gamma_n(i, m)$ and $\zeta_n(i, j)$ as defined in equations (7.20), (7.21) and (7.22), respectively, can be used to reestimate the model parameters from the observation sequence $F(n, N_0)$ and the initial model Λ. They have shown that the reestimated model parameters define a new model $\overline{\Lambda} = (\overline{\pi}, \overline{A}, \overline{B})$ which can either be the same as the initial model Λ or can have greater likelihood of the observation sequence $F(n, N_0)$, i. e., $P(F(n, N_0)|\overline{\Lambda}) \geq P(F(n, N_0)|\Lambda)$. The model parameters can be updated by iteratively replacing the initial model Λ by the new model $\overline{\Lambda}$ to increase the likelihood of the given observation sequence $F(n, N_0)$ till

a limiting point at which there is no significant gain in the likelihood. This procedure of parameter reestimation from a given observation sequence and the initial model is known as Baum-Welch reestimation method [106]. The reestimation formula due to this method for prior state probability π_i, state transition probability a_{ij} and the mixture density parameters c_{jm}, $\underline{u}_{jm}$ and Σ_{jm} are

$$\overline{\pi}_i = \gamma_1(i), \tag{7.23}$$

$$\overline{a}_{ij} = \frac{\sum_{n=1}^{N_0-1} \zeta_n(i,j)}{\sum_{n=1}^{N_0-1} \sum_{m=1}^{\mathcal{M}} \gamma_n(i,m)}, \tag{7.24}$$

$$\overline{c}_{jm} = \frac{\sum_{n=1}^{N_0} \gamma_n(j,m)}{\sum_{n=1}^{N_0} \sum_{m=1}^{\mathcal{M}} \gamma_n(j,m)}, \tag{7.25}$$

$$\overline{\underline{u}}_{jm} = \frac{\sum_{n=1}^{N_0} \gamma_n(j,m) \cdot G(n)}{\sum_{n=1}^{N_0} \sum_{m=1}^{\mathcal{M}} \gamma_n(j,m)}, \tag{7.26}$$

$$\overline{\Sigma}_{jm} = \frac{\sum_{n=1}^{N_0} \gamma_n(j,m) \cdot (G(n) - \underline{u}_{jm})(G(n) - \underline{u}_{jm})^T}{\sum_{n=1}^{N_0} \sum_{m=1}^{\mathcal{M}} \gamma_n(j,m)}. \tag{7.27}$$

Following the details of HMM provided above, we represent each BMA class through an HMM for the classification purpose. Let us add a subscript k to the notations as defined above to define the HMM for k^{th} BMA class as $\Lambda_k = (\underline{\pi}_k, A_k, B_k)$. If a total of c different BMA classes are used to form a classifier then $1 \leq k \leq c$. A part of the set of feature sequences $F(n, N_0)$ defined in Section 7.3.2 for each BMA is reserved for training purpose. For k^{th} BMA class these training sequences will be indicated as $F_k(n, N_0)$. We train the HMM representing k^{th} BMA class using the training data $F_k(n, N_0)$. In this training, the parameters of all the HMM $\Lambda_k,\ 1 \leq k \leq c$ are derived in order to maximize the likelihood of their corresponding training sequences $F_k(n, N_0),\ 1 \leq k \leq c$ using the Baum-Welch method [106] described above

$$\Lambda_k = \arg\max_{\Lambda} P(F_k(n, N_0)|\Lambda),\ 1 \leq k \leq c. \tag{7.28}$$

The parameters $\Lambda_k,\ 1 \leq k \leq c$, obtained after this supervised training will be used for classification of feature sequences reserved for the testing purpose.

7.3.4 Activity Classification

We have seen that in a BMA classifier each of the specified BMA is represented by an HMM having its parameters obtained by the given supervised training using the features from the motion artifact signal. Let c be the number of models corresponding to c different BMA classes and a feature sequence $F(n, N_0)$ is provided for testing, which belongs to any of the c BMA classes indexed by $k = 1, 2, \ldots, c$. It is possible to find the likelihood of the given test

sequence $F(n, N_0)$ for being in any of the c BMA classes. Let us denote the likelihood of $F(n, N_0)$ computed using the k^{th} model corresponding to the k^{th} BMA class, with parameters $\Lambda_k = (\underline{\pi}_k, A_k, B_k)$ as $P(F(n, N_0)|\Lambda_k)$. The BMA class can be recognized using the criterion of the maximum likelihood

$$u = \arg \max_{k,\ 1 \leq k \leq c} P(F(n, N_0)|\Lambda_k), \tag{7.29}$$

where u is the label of the recognized BMA class out of the possible $k = 1, 2, \ldots, c$ indices. The given test sequence is now classified to an appropriate BMA class.

7.4 Experimental Results

7.4.1 PCA-based Recognition

The collected ECG data from the subjects is analyzed using the PCA-based technique. The results of the PCA-based analysis are presented here in this section. First, the results of BMA classification in terms of classification rates, accuracy and false alarms are presented. This includes single subject classifiers with subject specific training and multiple subjects classifiers with combined training. Different classifiers are formed using different combinations of BMA classes that we will explain in this section. In the second part, we present an example of motion artifact removal using the class specific PCA-based filtering of the ECG signal. The improvement due to the PCA-based filtering is shown through better localization of detected P and T waves.

BMA Classification

A uniform length of 160 sample point duration is chosen for each ECG beat during the preprocessing steps. The BMA label (ground truth) is known for each of the ECG beats collected. The data set is divided into two parts: one for training the classifiers and the other for classifier testing purposes. The exact details of the population size for each of these two parts for various BMAs are given in Table 7.1. The column 'Single Subject' corresponds to the case where the classifier is trained for a particular subject (subject number one in our experiment) and tested on the same subject. The last column corresponds to the case when the classifier is both trained and tested for a collective pool of subjects and not specific for a single subject. The known BMA labels in the test data are used for performance evaluation of the classifier testing and are not available to the classifier itself. The classification test is performed on the sequences of 30 consecutive ECG beats (30×160 sample points).

The performance is evaluated based on two parameters: accuracy (P_T) defined as

$$P_T = N_{true}/(N_{true} + N_{missed}), \tag{7.30}$$

Table 7.1. Details of number of ECG beat streams used for training and testing of a particular BMA.

Body movement activity	Single Subject		Multiple Subjects	
	training	testing	training	testing
Sitting still	289	578	2927	5854
Left arm	227	454	2336	4672
Right arm	278	557	2278	4556
Both arms	224	449	1586	3112
Walking	583	1167	4120	8240
Twisting	355	711	2798	5597
Climbing down	268	536	1407	2814
Climbing up	344	688	1879	3759
Total	2568	5140	19331	38604

and false detection rates (P_F) defined as

$$P_F = N_{false}/(N_{true} + N_{false}), \tag{7.31}$$

where N_{true} is the number of true detections, N_{missed} is the number of missed detections and N_{false} is the number of false detections.

We use the following example to explain this. A classifier has three classes namely A1, A2 and A3 and the corresponding number of test signals recorded are 100, 90 and 80. Now, if the classifier detects 95 test signals as class A1 and 10 out of these 95 detections, actually belong to either class A2 or class A3 rather than class A1, then $N_{false} = 10$, $N_{true} = 95 - 10 = 85$ and $N_{missed} = 100 - 85 = 15$.

A hierarchical tree structure of BMA classes is shown in Fig. 7.6. There are five BMA classes in the top layer: (1) sitting still, (2) arm movement, (3) walking and climbing down stairs (W&CD), (4) climbing upstairs and (5) twisting movement at waist. The arm movement is a combined class of three separate movements of (2a) left arm, (2b) right arm and (2c) both arms. Similarly, W&CD is a combination of two BMA subclasses: (3a) walking and (3b) climbing down stairs. These BMA subclasses, shown in the second layer of the graph, demonstrate partial correlation among the corresponding motion artifacts. As a result these subclasses are subject to more false detections. To study this aspect of BMA classification in ECG signals, we construct five different types of BMA classifiers (Table 7.2) formed by various possible combinations of BMA classes/subclasses (Fig. 7.6).

Since an artifact subspace in the given scheme of BMA classification is represented by a corresponding set of eigenvectors, the performance of the classifiers is studied against the number of eigenvectors used to represent the subspace. Fig. 7.7 shows the performances of the classifiers I-V that are trained and tested on data collected from a single subject. Here the training is very specific to an individual subject and the performance shown here is

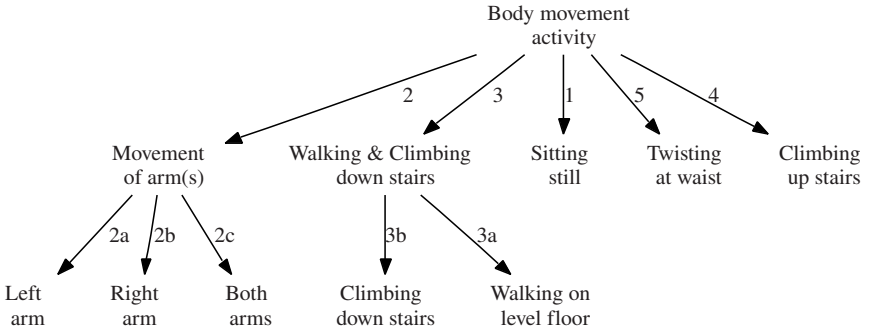

Fig. 7.6. Various BMAs and possible class formation by combining two or more BMAs into a single class. (©2007 IEEE)

Table 7.2. Five different classifiers for subject specific training with various combinations of BMA classes / subclasses in Fig. 7.6. The corresponding classifiers for multiple subjects are VI to X.

Classifier		BMA
Subject specific	Subject independent	
I	VI	1, 2, 3 and 4
II	VII	1, 2, 3a, 3b and 4
III	VIII	1, 2a, 2b, 2c, 3 and 4
IV	IX	1, 2a, 2b, 2c, 3a, 3b and 4
V	X	1, 2a, 2b, 2c, 3a, 3b, 4 and 5

also specific to the same subject. It is noted that the accuracy improves as the number of eigenvectors is increased from one to six, which results in a wider span of the artifact subspace of an individual BMA class. However, the performance saturates with further increase in the number of eigenvectors, since this results in overlapping of the spanned subspaces for different classes.

Due to possible correlation among the eigenfunctions of the specified subclasses, there is a drop in accuracy with increasing number of classes. The P_T value for classifier I (4 classes) is 98%, whereas for classifier V (8 classes) P_T = 85%. Thus it is possible to accurately recognize the BMA from the ambulatory ECG itself, but the degree of accuracy depends on separability of the BMAs.

The complete performances of the above BMA classifiers I, II, III and IV are presented in Fig. 7.8(a), 7.8(b), 7.8(c) and 7.8(d), respectively, showing the confusion matrix for all classes. In all cases six eigenvectors are used for the classification of the data collected from a single subject. In classifier I there are four BMA classes: 1, 2, 3, and 4 (Table 7.2). The accuracy P_T of the classifier I is 98% with a false detection rate P_F=1.4%. This suggests that

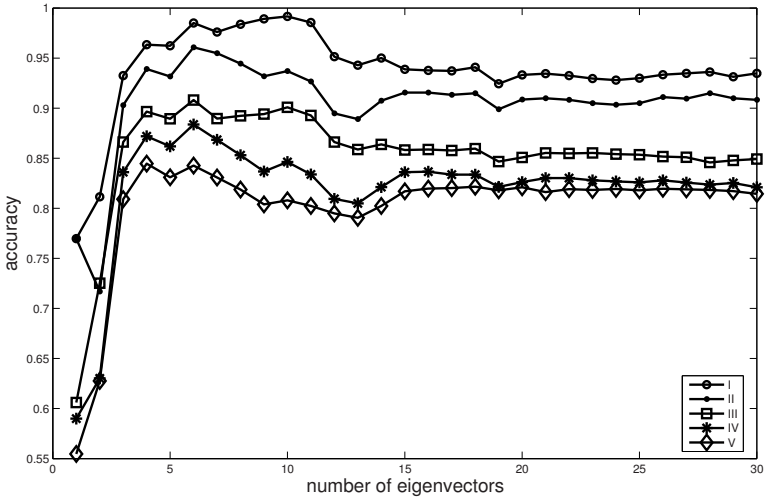

Fig. 7.7. Classification accuracy as a function of number of eigenvectors for the BMA classifiers: I, II, III, IV and V. (©2007 IEEE)

all these four classes of BMAs are very well separable using the PCA-based classification technique.

In BMA classifier II, there are five BMA classes: 1, 2, 3a, 3b, and 4. Here, the activities of walking (3a) and climbing down (3b) stairs are recognized as separate classes. However, there is a moderate amount of confusion between these two classes: 3a and 3b, as shown in Fig. 7.8(b), about 18% of total known labels of climbing down stairs are misclassified as walking and 4% of walking labels are misclassified as climbing down stairs. For these two classes, the average $P_T = 90\%$ and $P_F = 8.5\%$. The average performance for classifier II is $P_T = 96\%$ and $P_F = 4\%$. Further studies will be required to determine if there is a fundamental limitation in separating walking and climbing down. A possible explanation suggests that the corresponding gaits for these two BMAs differ only in the lower limbs and the upper body gait remains similar during both the activities. It is only the upper body gait that matters in generating a particular type of motion artifact.

In BMA classifier III there are six BMA classes: 1, 2a, 2b, 2c, 3, and 4. Here, the movement of left arm (2a), right arm (2b) and both arms (2c) are recognized as separate classes. However, a significant level of confusion exists between these three classes as shown in Fig. 7.8(c). On average, 25% of total known labels of both the classes 2b and 2c are misclassified as 2a, and 12% of total known labels of the 2b are misclassified as 2c. For these three classes, average P_T is 77% and P_F is 17%. The average performance for classifier III is $P_T = 91\%$ and $P_F = 7\%$. This suggests that, for the given

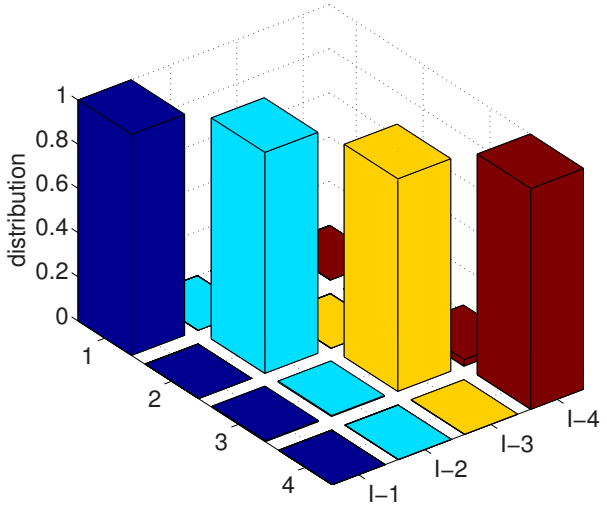

(a)

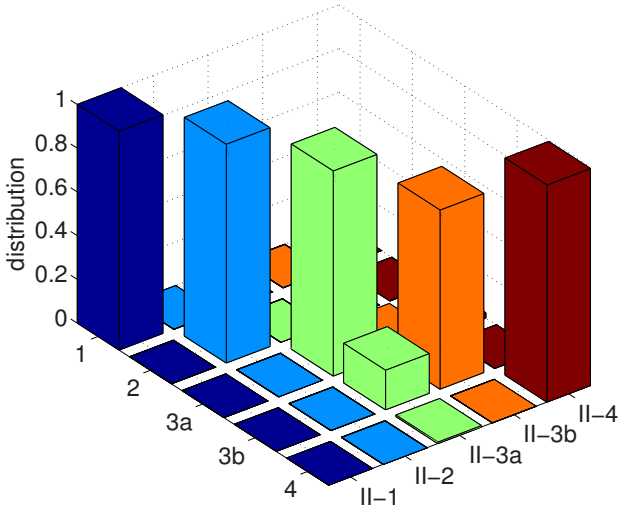

(b)

(See next page for figure caption.)

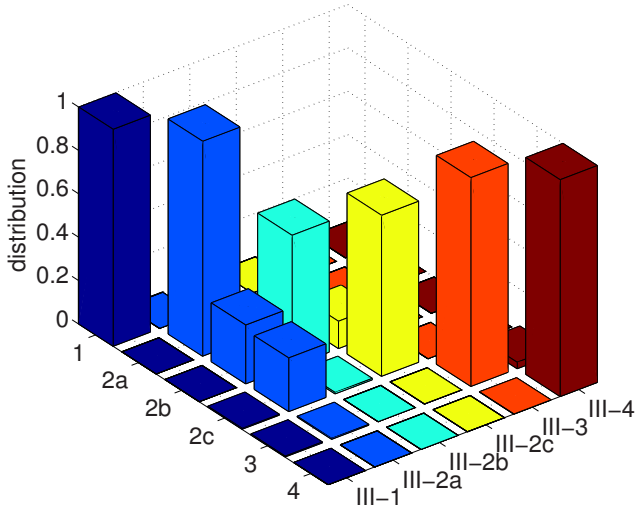

(c)

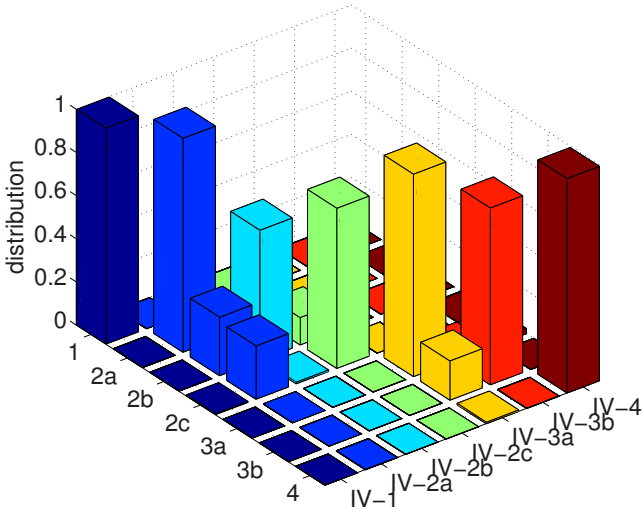

(d)

Fig. 7.8. Confusion matrices for BMA detection for classifiers (a) I, (b) II, (c) III and (d) IV. The horizontal axes in each case represent known and recognized BMA classes. The vertical bars represent the classification accuracy. (©2007 IEEE)

lead-II configuration, any movement of the arms (be it left or right) does affect the ECG signal in a similar manner which reduces the differentiability of the corresponding BMAs.

In BMA classifier IV, there are seven BMA classes: 1, 2a, 2b, 2c, 3a, 3b, and 4. Here the BMA (2a) left arm, (2b) right arm and (2c) both arms movement, (3a) walking and (3b) climbing down stairs are recognized as separate BMA classes. The notable aspect about the classifier IV is that all the seven different BMA classes are recognized by a single classifier. The confusion levels between classes are similar to that of classifier III (arm movements) and classifier II (walking and climbing down stairs). The classifier IV demonstrates $P_T = 88\%$ and $P_F = 10\%$, which is worse than the previous cases, due to the larger number of classes considered.

In BMA classifier V, there are now eight BMA classes: 1, 2a, 2b, 2c, 3a, 3b, 4 and 5. As compared to the classifier IV, the performance under the BMA subclasses 2a, 2b and 2c is further deteriorated since a new BMA class of twisting at waist introduced here also involves arm movement. The classifier V has $P_T = 84\%$ and $P_F = 13\%$.

The results given so far (Fig. 7.8) correspond to analyzing the performance of the classifiers on a single subject (subject number one in this case). We now compute the inter-subject variability of the obtained results by computing the classification rates for each classifier trained and tested on individual subjects. This is given in Table 7.3 for the classifiers I-V. It can be seen from the table that the mean accuracy (P_T) and mean false detection rate (P_F) for these classifiers display similar behaviors as discussed earlier. The standard deviation for accuracy is quite low. However, the standard deviation for the false detection rates appears to be on a slightly higher side.

Table 7.3. Inter-subject variability of classification rates (in %) of the subject-specific classifiers over the entire subject population.

Classifier	Accuracy (P_T)		False detection rate (P_F)	
	mean	std. dev.	mean	std. dev.
I	92.44	6.71	5.95	5.38
II	86.81	8.38	9.78	6.64
III	79.85	7.11	15.23	5.52
IV	73.98	8.97	19.06	6.53
V	72.79	7.51	20.20	6.08

The results presented above were for the classifiers I to V, tested with subject specific training. The subject specific training allowed us to shield the classifier from possible inter-personal variability. Hence we now repeat the experiments where principal components are learnt not from an individual subject, but from all subjects available with us. The corresponding classifiers VI to X (see Table 7.2) are trained on 23 different subjects to understand the

impact of inter-personal variability on classifier performance. As mentioned earlier, one third of the available ECG beats from each subject but pooled together to form a common pool of training data have been used for training purposes. The accuracy of classification for various choices of the number of eigenvectors is plotted for the classifiers VI to IX in Fig. 7.9. As compared to the training over a single subject the required number of eigenvectors is much higher and the maximum P_T is only 85%, as expected. The confusion matrices of the classifiers VI to IX using 19 eigenvectors are plotted in Fig. 7.10. The trends of confusions among certain classes, i.e. arm movement classes or walking and climbing down stairs, are similar to that in the subject specific classifiers.

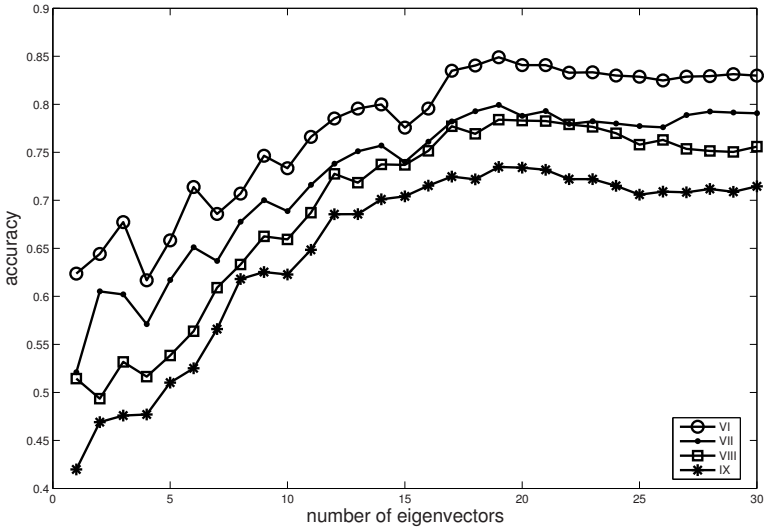

Fig. 7.9. Accuracy of the combined (multi-subject) classifiers as a function of number of eigenvectors used to represent the artifacts when the data is collected from different subjects. Here the classifiers are VI, VII, VIII and IX. (©2007 IEEE)

To study further the effect of inter-personal variation in ECG data, a new classifier, called classifier XI with four BMA classes 1, 2, 3, and 4 is trained on 22 subjects out of the total 23 subjects, leaving each time one designated test subject. This is equivalent to employing a leave-one-out testing method. The performance of classifier X is $P_T(\text{max.})= 72\%$ and $P_F(\text{min.})= 26\%$. Thus, it appears that the error signal generated due to inter-personal variation is significant. It is therefore advisable that the classifier be customized for a given user in order to achieve the highest accuracy. However, this should not be a cause of alarm as the W-ECG system is meant to monitor only a specific

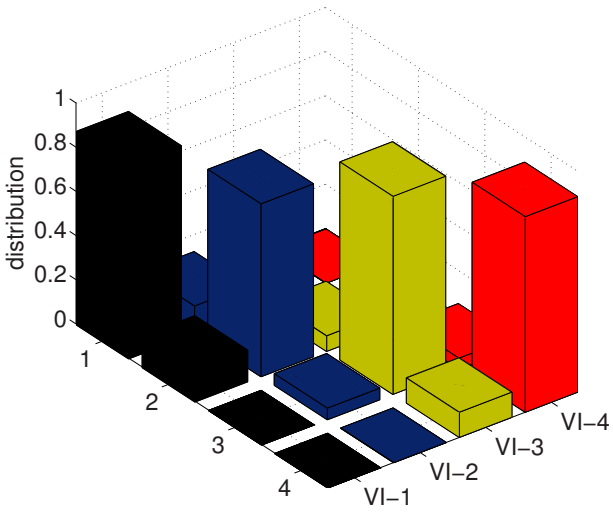

(a)

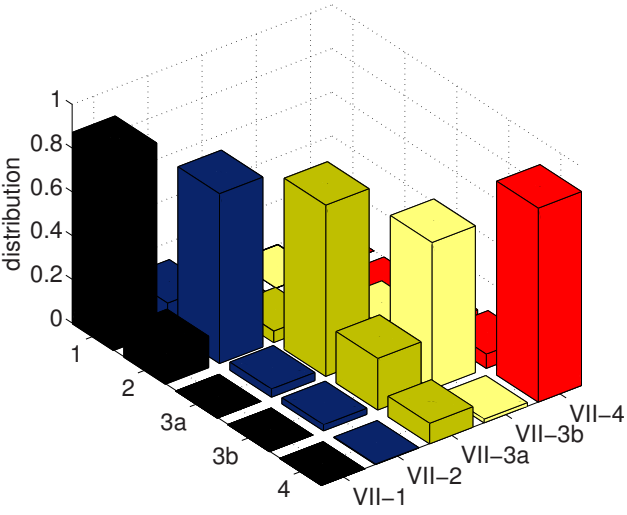

(b)

(See next page for figure caption.)

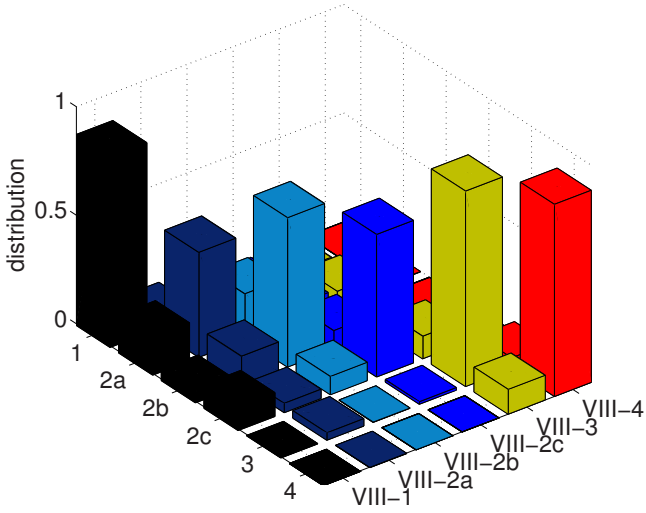

(c)

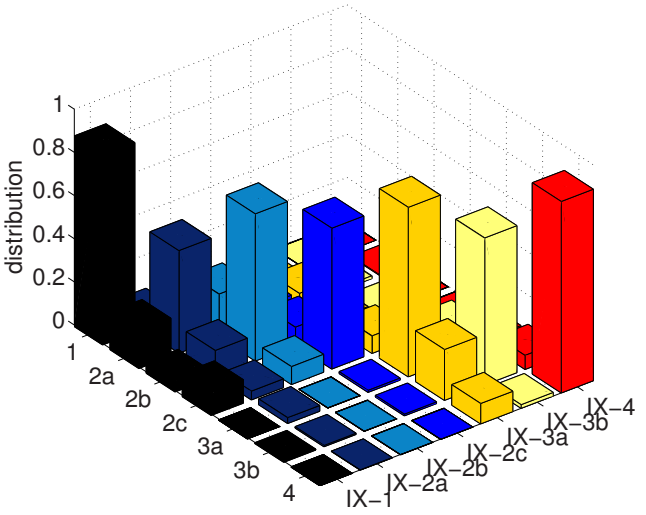

(d)

Fig. 7.10. Confusion matrices for BMA detection for multi-subject classifiers (a) VI, (b) VII, (c) VIII and (d) IX. The horizontal axes in each case represent known and recognized BMA classes.

subject at a given time. Hence it should be possible to retrain the classifier for each subject.

Detection of P and T Waves in Presence of BMA

Fig. 7.11(a) shows a sequence of recorded ECG beats in presence of BMA (walking) prior to artifact removal. In Fig. 7.11(b) the component due to motion artifacts as derived by the class specific PCA-based method using the classifier III is shown. In Fig. 7.11(c) the reconstructed ECG signal after subtracting the artifact signal is shown. The ECG signal after the removal of motion artifacts is quite clean even though this has been accomplished with a single lead W-ECG.

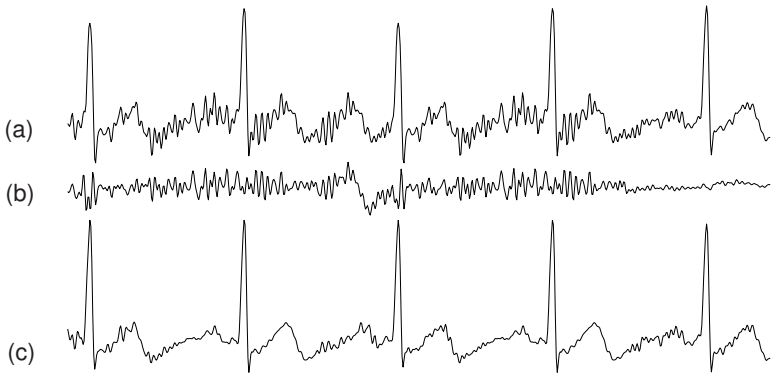

Fig. 7.11. Illustration of artifact removal from ambulatory ECG using the class specific PCA-based filtering. (a) Original ECG signal before any artifact removal, (b) artifact signal derived by the class specific PCA-based method, and (c) reconstructed ECG signal after subtracting the artifact signal. (©2007 IEEE)

This artifact removal procedure helps to improve the quality of analysis of ECG signal in presence of BMA as demonstrated here in the detection of P and T waves in the collected ECG data. The P wave is a small and smooth peak that occurs just before the QRS complex due to atrial activity of the heart and the T wave occurs following the QRS complex due to the ventricular activity. In order to detect the P, QRS complex and T waves, we use a combination of two existing techniques in the literature [63, 66, 132]. First, the ECG signal is smoothed by a low-pass filter with a 3dB cut-off at 12Hz as recommended in [66] for P and T wave detection. Then a morphological operator for detecting P and T waves is applied which is inspired by the method

of QRS detection in [132]. Since the R peak position is in the middle, P and T waves are located by searching for maxima in the appropriate windows before and after the R peak position in the output of the morphological filter.

The histograms representing the locations of P and T waves detected in the ECG signal from a particular subject (a part of the ECG is shown in Fig. 7.11), before and after artifact removal, are shown respectively in Fig. 7.12(a) and 7.12(b). It may be noted that since the input beats have already been resampled to have the same number of samples, the samples may correspond to different timings based on the resampling factor used earlier. In order to plot them on an actual time unit, the locations of the detected P and T waves are shown after correcting for the resampling operation. In Fig. 7.12(a), the histogram without the artifact removal is broadly spread out (standard deviations of 46.4ms and 29.8ms, respectively, for P and T locations) while in Fig. 7.12(b) the histogram is much narrower (standard deviations of 8ms and 11.9ms, respectively, for P and T locations). It is noted that a 12Hz prefiltering is applied to the ECG signal in both the cases prior to detection of P and T waves. This shows that in the presence of BMA induced artifact, the 12Hz lowpass filter as suggested in [66] alone is not sufficient for the accurate localization of P and T waves and the given artifact removal scheme improves the quality of analysis.

7.4.2 HMM-based Recognition

Here we present the results of HMM-based BMA recognition from the ambulatory ECG signal. The 'sitting still' is considered here as a representative class of the ECG data for which there in no BMA present and hence it is free from any motion artifact. This signal is taken as the representative of the reference signal while using the adaptive filter proposed earlier to estimate the component due to the cardiac cycle in presence of motion artifact. The methodology explained in the previous section is adopted for training various BMA classifiers with different combinations of BMA classes as listed in Table 7.2. Here we concentrate only on the subject specific cases only.

We use 80% of the available data for each individual subject for training purposes, and the remaining 20% of the data is used for testing purposes.

First, we explore the HMM-based method for BMA recognition for testing the accuracy of classification with subject specific training. The BMA classifiers I to V as described in Table 7.2 are trained using the data from an individual subject. The following set of parameters is used in the feature extraction step: α=1.5, f_0=1Hz, L=10, and W=484 (equivalent to 2s of the data length at f_s=242Hz). The classifiers are trained using the appropriate number of HMMs using the supervised learning method given in Section 7.3.3. The number of states $\mathcal{Q}$=4 and number of mixture components $\mathcal{M}$=3 are chosen for this experiment. The trained classifiers are used for recognition of BMA from the test sequences collected from the same subject according to the technique given in Section 7.3.4. Here the length of each test sequences is chosen to

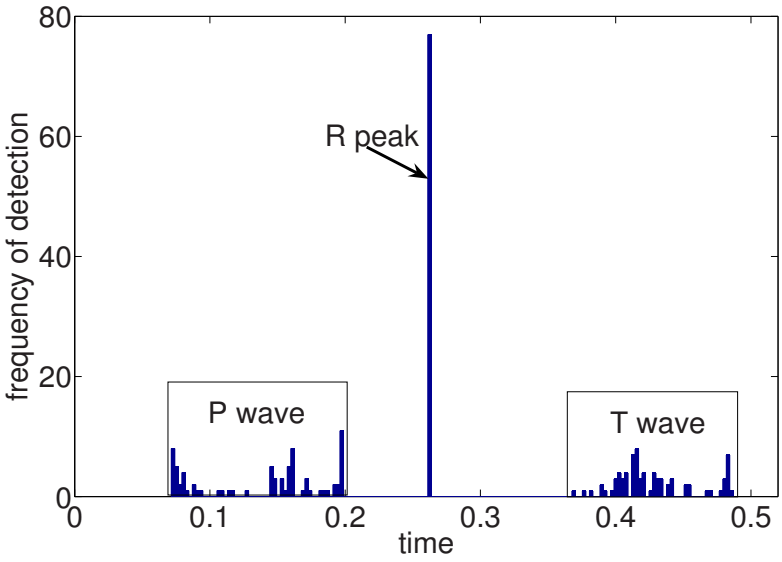

(a)

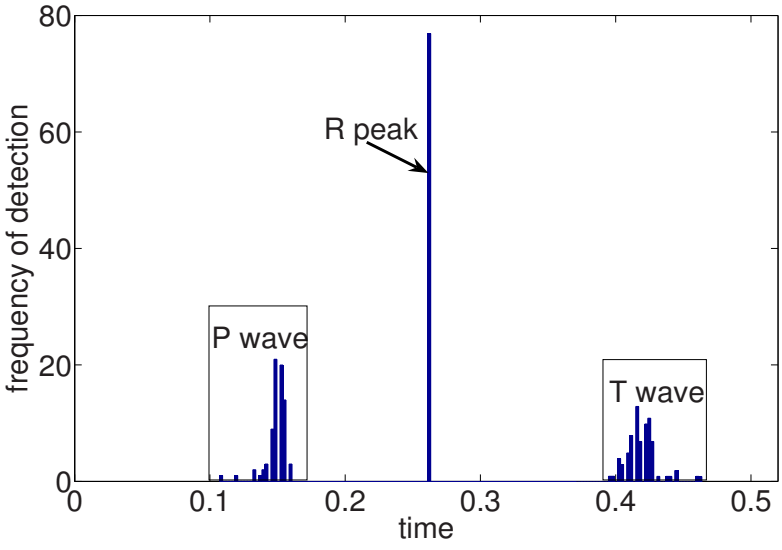

(b)

Fig. 7.12. Histograms of location estimates of P and T waves with respect to the location of R wave (a) when motion artifacts were present and (b) after artifact removal. The horizontal axes represents actual time in seconds. (©2007 IEEE)

be N_0=1200 (approximately equivalent to 5 seconds of ECG recording). The accuracy of classification P_T is calculated using Eq. (7.30). This experiment of the subject specific training is repeated for all subjects individually and with the same parameter values as described above. The aggregate of confusion matrices for classifiers I to IV, showing the accuracy of the classifier as well as amount of misclassification to other classes over the actual vs. recognized BMA classes are presented in Fig. 7.13 for these experiments for the subject specific training. The confusion matrix for the classifier I with subject specific training is shown in Fig 7.13(a). There are four BMA classes in the classifier I: 1. sitting still, 2. movements of arm(s), 3. walking on level floor and climbing down on stair combined (W&CD), and 4. climbing up stairs. There are two most significant confusions: 5.3% of 'sitting still' are recognized as movement of arm(s) and 4.6% of climbing up stair are recognized as W&CD. Most of the other confusions among the BMA classes are much less than 1%. The aggregate accuracy of this classifier is 97.6%.

The confusion matrix for the classifier II with subject specific training is shown in Fig 7.13(b). There are five BMA classes in the classifier II : 1. sitting still, 2. movements of arm(s), 3a. walking on level floor, 3b. climbing down on stair, and 4. climbing up stairs. Here the two BMA classes indicated as 3a and 3b, are separated as opposed to the classifier I in which they were combined into W&CD class. The most significant confusion occurs at 5.6% of the climbing down stairs being recognized as walking on level floor, which is expected because of the similarity of the two BMAs. The aggregate accuracy of this classifier is 97.1%.

The confusion matrix for the classifier III with subject specific training is shown in Fig 7.13(c). There are six BMA classes in this classifier. Here three BMA classes are indicated as 2a, 2b and 2c, corresponding to the movements of left, right and both arm(s), respectively. Here 10% of each of the movements of left and right arm are recognized as movements of both arms. Apart from these, 10%, 3% and 6% of 2a, 2b and 2c, respectively, are recognized as W&CD. The result shows a significant difficulty in recognizing movements of left arm, right arm and both arms as three different classes. The aggregate accuracy of the classifier III is 92.3% which is substantially less than the previous two classifiers.

The confusion matrix for the classifier IV with subject specific training is shown in Fig 7.13(d). There are seven BMA classes in the classifier IV. Here the three movements of left, right and both arm(s) indicated as 2a, 2b and 2c, respectively, are separated along with 3a and 3b BMA classes. The types of confusions mentioned above for the classifiers II and III, are also seen in this classifier, hence the accuracy drops to 90.5%. However, this can be considered quite significant with a view of having the ability to classify so many BMAs as different classes using a single-lead of ECG.

In order to explore the ability of the BMA recognition scheme to handle a larger number of BMAs, we introduce one more class of twisting at waist

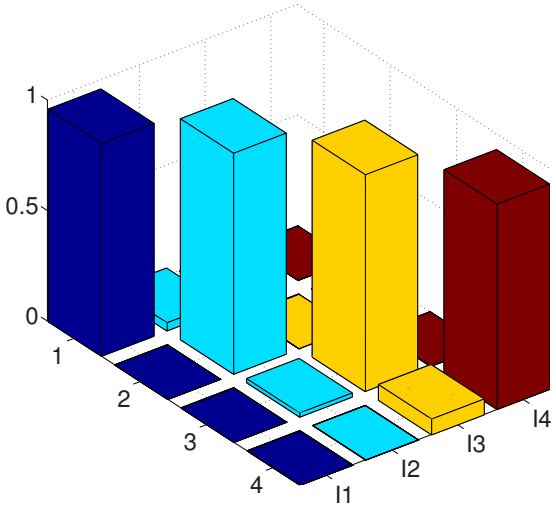

(a)

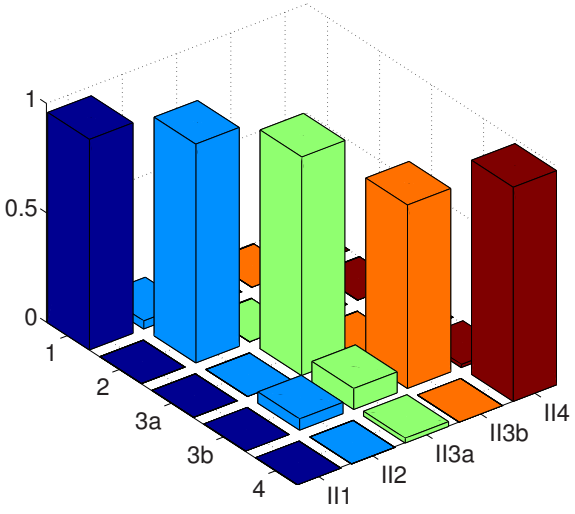

(b)

(See next page for figure caption.)

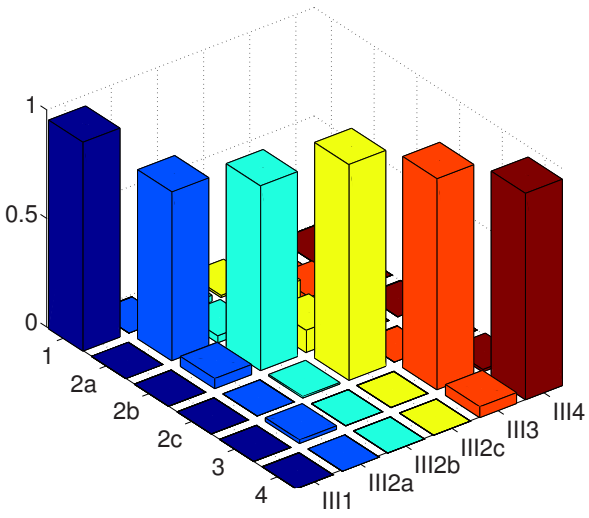

(c)

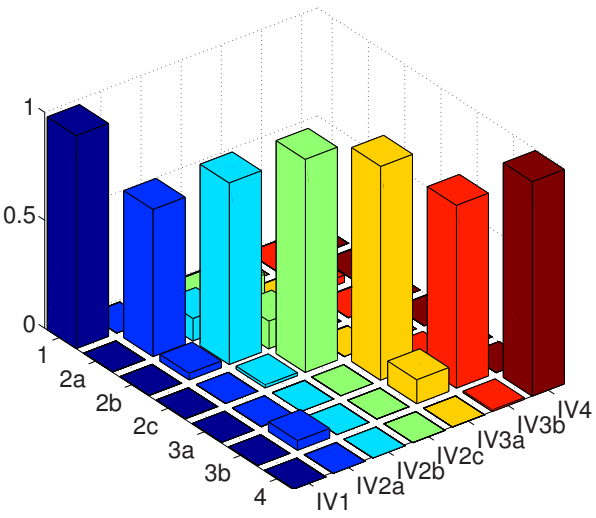

(d)

Fig. 7.13. Confusion matrices for BMA recognition using HMM for classifiers (a) I, (b) II, (c) III and (d) IV under subject specific training. The horizontal axes in each case represent known and recognized BMA classes. The notation IV2b means - class label 2b (right arm movement) for the classifier IV.

activity. The classifier V has eight BMA classes including the previously considered seven different BMA classes. The accuracy of the classifier V is 88.6%.

Table 7.4. Accuracies of BMA classifiers I to V for a single subject with different numbers of states and mixture components in HMM.

BMA Classifier	accuracy (%)			
	$\mathcal{Q}=3$, $\mathcal{M}=3$	$\mathcal{Q}=3$, $\mathcal{M}=4$	$\mathcal{Q}=4$, $\mathcal{M}=3$	$\mathcal{Q}=4$, $\mathcal{M}=4$
I	98.6	98.0	97.8	97.1
II	96.9	97.4	97.9	94.6
III	90.8	92.9	91.8	90.2
IV	92.2	91.5	89.8	88.9
V	91.9	90.2	89.1	89.8

Since we do not know exactly what are the best numbers of states and mixture components to choose for the HMM in the classifiers, we have selected the same combination of numbers of states and mixtures to represent each of the BMA classes. We have tried four different such combinations, e.g., ($\mathcal{Q}=3$, $\mathcal{M}=3$), ($\mathcal{Q}=3$, $\mathcal{M}=4$), ($\mathcal{Q}=4$, $\mathcal{M}=3$) and ($\mathcal{Q}=4$, $\mathcal{M}=4$), for all the five classifiers I to V. The remaining parameters are all as specified above for the subject specific classifiers I to V. The recognition accuracies for the classifiers I to V for the four different combinations of $(\mathcal{Q}, \mathcal{M})$ are presented in Table 7.4. We found that there in no further gain in terms of classification accuracy with more number of states or mixture components.

To verify the ability of classifiers I to V for handling inter-personal variability, a combined training over multiple subjects is provided to the corresponding multi-subject classifiers, VI to X. We train the classifiers using the training data collected from all the subjects. With this combined training the classifiers are tested against possible inter-personal variations in motion artifact signals for the same BMA. We had carried out similar experiments for PCA-based method also. The aggregate confusion matrices for the BMA classifiers VI to IX using HMM are shown in Fig. 7.14. Here also, like the subject specific training, the confusion takes place among the BMA classes of movements of left, right and both arm(s). Similarly, there are confusions taking place among walking and climbing up/down stairs classes. The classifiers VI to X for the combined subjects training have accuracies of 94%, 91.8%, 87%, 86.2% and 85%, respectively. It is observed, as in the previous case of PCA-based BMA classification, that the HMM-based method performs better if the subject specific training is provided. Though the accuracies obtained with the combined training as compared to those with subject specific training are on lower side, the deterioration in the HMM-based method is less than that using the PCA-based method discussed in the previous section.

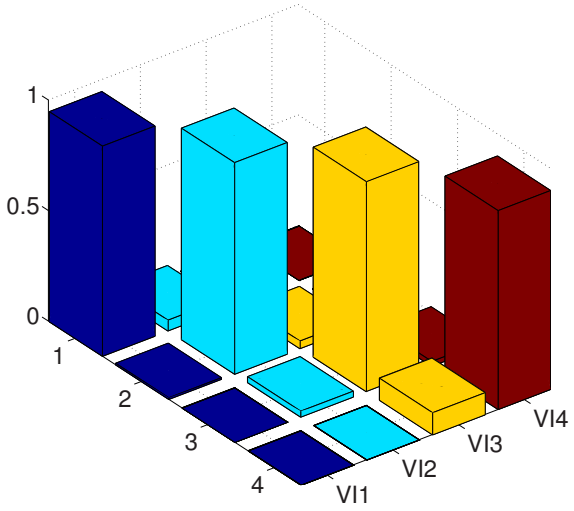

(a)

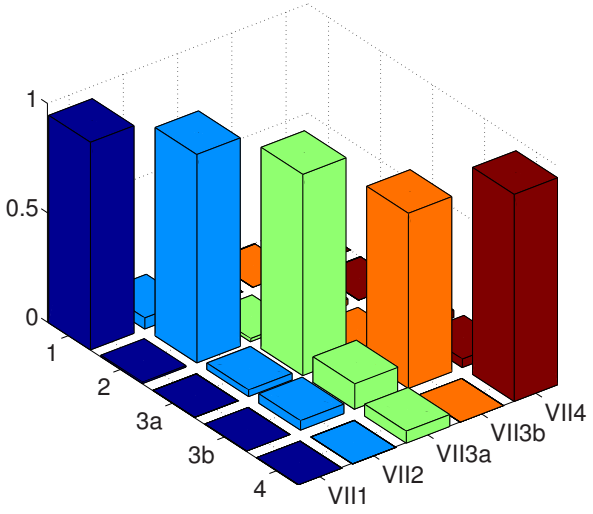

(b)

(See next page for figure caption.)

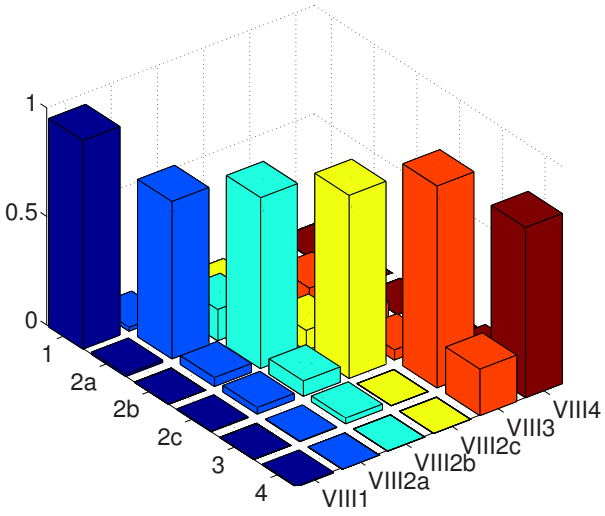

(c)

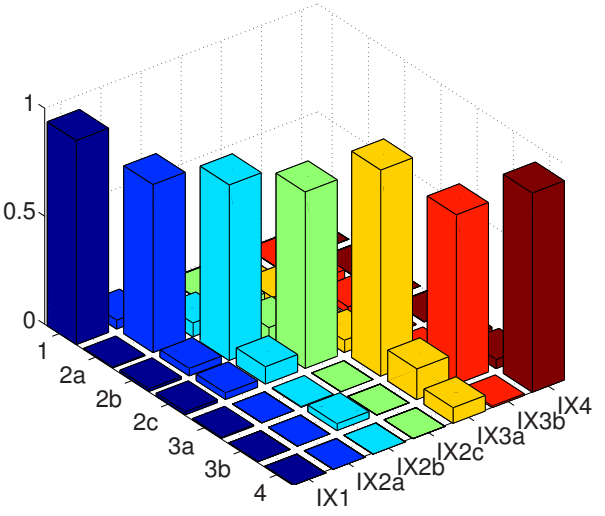

(d)

Fig. 7.14. Confusion matrices for BMA recognition using HMM for classifiers (a) VI, (b) VII, (c) VIII and (d) IX under combined training. The horizontal axes in each case represent known and recognized BMA classes.

In this chapter, we have discussed two techniques for BMA recognition from the motion artifacts in the ECG signal. Now we compare the accuracy of BMA classification for the HMM-based method with that of the PCA-based method. The average accuracies obtained on the data set considered in this experiment with the classifiers I to V are presented in Table 7.5 for both HMM-based and PCA-based methods. It is observed that the HMM-based method has higher accuracy of classification than that of the PCA-based method for all classifiers I to V and in both the cases with subject specific training and with combined training for all subjects. It is also noted that the standard deviation in the accuracy across the different individual subjects in case of subject specific training, is very small for the HMM-based method. Thus the HMM-based method is more consistent over the entire subject population. The comparison of accuracies with combined subjects training for both the techniques shows that the HMM-based technique works very well even with the inter-personal variations in the ECG. The HMM-based method is less sensitive to the inter-personal variations and it can handle such variation very well as opposed to the PCA-based method.

Table 7.5. Comparison of accuracies of BMA classifiers I to X for the subject specific (I-V) and combined (VI-X) training for PCA and HMM based methods. Accuracy for subject specific recognition is presented in terms of mean and standard deviation across all subjects.

method	accuracy (%)	BMA Classifier				
		I	II	III	IV	V
HMM-based subject specific	mean	97.1	96.7	91.8	89.9	88.0
	std. dev.	2.0	2.3	0.7	1.0	1.7
PCA-based subject specific	mean	93.7	88.8	82.5	77.4	75.1
	std. dev.	6.5	9.2	3.9	8.9	7.8
		VI	VII	VIII	IX	X
HMM-based subjects combined	mean	94.0	91.8	87.0	86.2	85.0
PCA-based subjects combined	mean	84.9	79.9	78.4	73.5	65.8

We have also analyzed the effect of the length of the test sequence $F(n, N_0)$ on the BMA recognition using the HMM-based classifiers. For all the classifiers I to V we find that the recognition accuracy improves with the increasing length of the test input from N_0=300 samples (≈1.24s) to N_0=1200 samples (≈4.96s). The mean accuracy across the subjects along with the vertical bars indicating the standard deviation versus the length of the test sequence is plotted in Fig. 7.15. In order to achieve a good accuracy of BMA classification using the HMM-based method a reasonable choice of length of the test sequence is found to be about 5s.

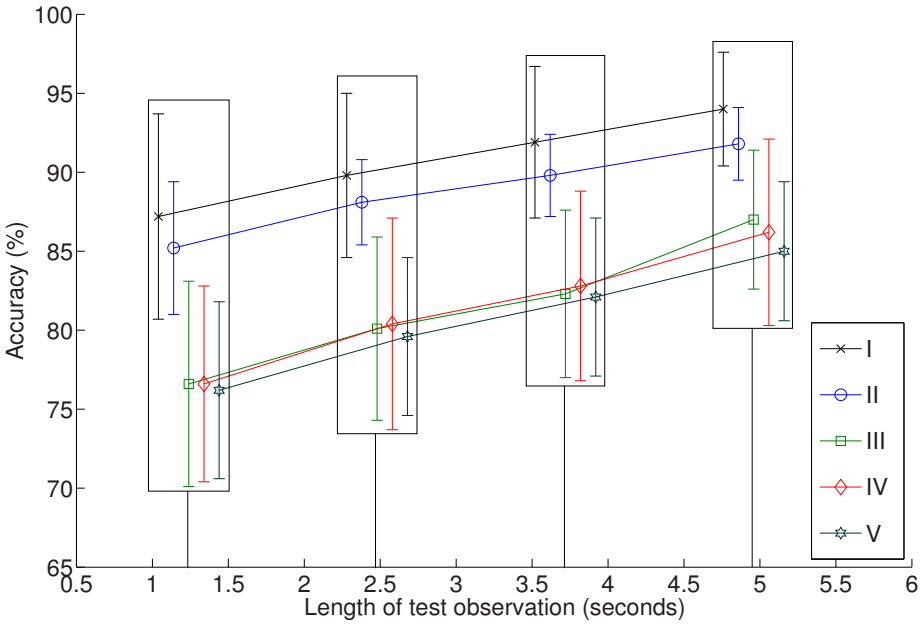

Fig. 7.15. Accuracy vs. length of the test sequence for the BMA classifiers I to V. Height of the vertical bars at each of the coordinates indicates one standard deviation above and below at that point. Five plots correspond to five different classifiers I-V.

7.5 Discussion

In this chapter we have studied classifiability of various BMAs like sitting still, movement of arms, walking and climbing stairs up and down, using the motion artifacts present in ECG signals. It is observed that different BMAs have different separations among them and this determines the accuracy of classification. For example, while climbing up stairs is recognized with a good accuracy ($P_T = 99\%$), there exists a moderate confusion between walking and climbing down stairs and a significant confusion among the movements of left, right and both arms. When we merge two overlapping classes such as walking and climbing down stairs into a single BMA class, the performance expectedly improves. It would be of interest to study the confusion level if the pace of walking/climbing downstairs is increased. Similarly, confusion levels in the case of vigorous arm movement will be of interest. Currently, we have refrained from such activities that may impose stress on the heart, a condition we wanted to preclude in this preliminary study on BMA recognition from motion artifacts.

The performance is the best when the classifier is provided subject specific training, meaning that personal training is recommended rather than generic training on multiple subjects.

In order to be able to use the given PCA-based method, we had to resort to resampling of the ECG beats to match the dimensionality, which may introduce certain artifacts in the QRS complex. Another possible option is to do zero padding to match the dimension. However, this would introduce artifacts in the signal representing BMA that is prevalent over the entire beat duration. In order to avoid that we suggested the use of HMM-based classification.

We have shown that the time localized spectral features of the motion artifact signal can be used for BMA recognition. We have achieved better recognition rates using the HMM-based method as compared to PCA-based method. We have also given a scheme using an adaptive filter for separating motion artifact signal from the ECG which can be used for the estimation of the cardiac cycles in the ECG signal contaminated by the motion artifact. We have found that a 5s long recording is ideal for BMA recognition. A smaller length of the data results in a reduced accuracy, while a longer length of the data will add to the system delay.

We have also experimented on the effect of varying the number of states and mixture components for the HMM. However, a much more elaborate evaluation is needed to ascertain what would be the correct HMM model for classification purposes.

For the given supervised learning technique, the available ground truth is in terms of labels that qualitatively describe activities (e.g. walking gently). However, a more precise labeling of BMA in terms of speed and rigorousness is likely to provide a better understanding of the impact of the resultant motion artifacts. This may be achieved by attaching a network of motion sensors to the body and recording the motion signals synchronously with the ECG signal. In the next chapter we will study the impact of levels of BMA on motion artifact generation quantitatively by using the ground truth from the acceleration signals captured from the moving body parts.